nature communications

Article

https://doi.org/10.1038/s41467-024-53396-x

# Sprayable inflammasome-inhibiting lipid nanorods in a polymeric scaffold for psoriasis therapy

Received: 3 March 2024

Accepted: 11 October 2024

Published online: 19 October 2024

Check for updates

Dhanashree Surve[1], Adam Fish[1,4], Maharshi Debnath[1,4], Aniruddha Pinjari[1], Adrian Lorenzana[1], Sumi Piya[2], Shelly Peyton[1] & Ashish Kulkarni[1,3]

Localized delivery of inflammasome inhibitors in phagocytic macrophages could be promising for psoriasis treatment. The present work demonstrates the development of non-spherical lipid nanoparticles, mimicking pathogen-like shapes, consisting of an anti-inflammatory inflammasome inhibiting lipid (pyridoxine dipalmitate) as a trojan horse. The nanorods inhibit inflammasome by 3.8- and 4.5-fold compared with nanoellipses and nanospheres, respectively. Nanorods reduce apoptosis-associated speck-like protein and lysosomal rupture, restrain calcium influx, and mitochondrial reactive oxygen species. Dual inflammasome inhibitor (NLRP3/AIM-2-IN-3) loaded nanorods cause synergistic inhibition by 21.5- and 59-folds compared with nanorods and free drug, respectively alongside caspase-1 inhibition. The NLRP3/AIM-2-IN-3 nanorod when transformed into a polymeric scaffold, simultaneously and effectively inhibits RNA levels of NLRP3, AIM2, caspase-1, chemokine ligand-2, gasdermin-D, interleukin-1β, toll-like receptor 7/ 8, and IL-17A by 6.4-, 1.6-, 2.0-, 13.0-, 4.2-, 24.4-, 4.3-, and 1.82-fold, respectively in psoriatic skin in comparison to Imiquimod positive control group in an in-vivo psoriasis-like mice model.

Psoriasis is a chronic inflammatory disease affecting 125 million people worldwide and was evaluated as high in the global burden of disease study[1]. Psoriasis is associated with increased inflammatory arthritis, and metabolic disorders, and affects mental health substantially[1,2]. Psoriasis involves the development of hyperkeratosis, vascular hyperplasia, and infiltration of immune cells[3,4]. The keratinocytes are responsible for the initiation and maintenance phases of psoriasis[5]. External stimuli expedite stressed keratinocyte formation and instigate the conversion of plasmacytoid dendritic cells (pDC) to myeloid dendritic cells (mDC) in the presence of inflammatory cytokines, including tumor necrosis growth factor alpha (TNF-α), interleukin-1-beta (IL-1β), and interferons (IFNα/γ)[5]. The activated keratinocytes release chemokines, including chemokine (C-X-C motif) ligand 1/2/3 (CXCL1/2/3) and C-C motif chemokine ligand 2 (CCL2), to recruit leukocytes like T cells (adaptive immune cells), dendritic cells, and macrophages to induce innate immunity[5]. Also, nucleotide-binding domain, leucine-rich-containing family, pyrin-domain-containing-1 (NLRP1), nucleotide-binding domain, leucine-rich-containing family, pyrin-domain-containing-3 (NLRP3), absent in melanoma 2 (AIM2) inflammasomes, nuclear factor kappa-light-chain-enhancer of activated B cells (NF-κB), and Gasdermin-D have been shown to aggravate psoriasis[6–9]. Vitamin D3 derivatives[10], immunosuppressants[11], anti-inflammatory small molecules and biologics[12], steroids[13], retinoids[14], and phototherapy[15] are currently administered to treat psoriasis. However, these treatments suffer from drawbacks, including chronic and acute systemic intoxication, tachyphylaxis, localized irritation, pustulation, skin atrophy, striations, telangiectasias, and diminished potency[13,16].

The inflammasome is a cluster of cytosolic proteins that are activated due to the oligomerized pathogen recognition receptors

[1]Department of Chemical Engineering, University of Massachusetts, Amherst, MA 01003, USA. [2]Pathology Department, University of Massachusetts-Chan Medical School, Baystate Medical Center, Springfield, MA 01199, USA. [3]Center for Bioactive Delivery, Institute for Applied Life Sciences, University of Massachusetts, Amherst, MA 01003, USA. [4]These authors contributed equally: Adam Fish, Maharshi Debnath. e-mail: akulkarni@engin.umass.edu

(PRR), including the nucleotide-binding domain and leucine-rich-repeat containing family (NLR) or absent in melanoma-2 (AIM2) like receptor (ALR) when encountered with the damage-associated molecular patterns (DAMP) or pathogen-associated molecular patterns (PAMP). It involves the formation of a protein complex with the pyrin domain of apoptosis-associated speck-like protein (ASC), the DAMP/PAMP, and the NLR/ALR. The protein complex activates caspase-1 downstream, releasing inflammatory cytokines and pyroptotic cell death[17,18]. The pathogen- and host-derived triggers stimulate canonical NLRP3 inflammasomes, unlike other NLR-based inflammasomes. The NLRP3 and AIM2 inflammasomes are also expressed by proliferating keratinocytes within psoriatic skin. However, the role of macrophages in the long-term persistence of psoriasis inflammation locally and systemically is gravely neglected. The persistence of psoriatic lesions is majorly caused due to significantly higher expression of macrophage inducible C-type lectin (mincle) associated with pro-inflammatory macrophages (M1)[19]. Prokineticin-2 (PK2) is a neuroendocrine peptide associated with psoriatic skin[5,20]. The PK2 activates NLRP3 inflammasomes in macrophages as an innate immune response, releasing IL-1β and exacerbating keratinocyte proliferation angiogenesis and psoriatic lesions[20,21]. Macrophages are key players in sensing the IL-1β and maintaining the PK-2-IL-1β positive feedback loop[20]. The tissue-resident macrophages (Langerhans cells) exist as a lineage from bone marrow from which the majority are lost due to disappearance reactions during the initial stages of the disease. Later, constant proliferation of remaining Langerhans cells occurs in response to persistent psoriatic inflammation[22]. The tissue-resident macrophages are present since birth and multiply due to local triggers (DAMP/PAMP) instead of recruitment from the blood circulation, unlike the dendritic cells[22]. Blood monocytes sense the inflammatory cytokine and circulate systemically causing vasculitis[22,23]. Therefore, it is vital to stop the proliferation of the long-ignored tissue-resident macrophages to attenuate local inflammation. Given their enhanced activity and role in the pathogenesis of psoriasis, attenuating inflammasome activation within macrophages would serve as a unique therapy for psoriasis treatment. However, existing inflammasome inhibitors lack specificity, potency, and ability to cross the hydrophobic stratum corneum, reducing efficacy[24]. Additionally, simultaneously targeting and inhibiting multiple types of inflammasomes could lead to enhanced efficacy against psoriasis. Nanoparticles have been utilized to enhance the cellular delivery of drugs for inflammatory diseases[25,26]. Recently, hyaluronic acid nanoparticles were demonstrated to possess an anti-psoriatic effect[27]. Various synthetic or plant extracts inhibiting NLRP3/AIM2 inflammasome were also explored against psoriasis[28–32]. However, the inhibitors and the hyaluronic acid nanoparticles would elicit systemic immunosuppressive effects due to intravenous or intragastric administration or be water soluble and may not penetrate the stratum corneum.

Lipid nanoparticles (LNPs) have been explored for topical delivery of drugs for psoriasis treatment[33,34]. However, recent reports demonstrated that LNPs consisting of phosphatidylcholine and PEGylated lipids, with or without cationic and ionizable lipids, activate inflammasomes or the immune response[35,36]. Studies have also explored the effect of physicochemical properties of nanoparticles, including particle size, zeta potential, and formulation composition, on NLRP3 inflammasome activation[37,38]. There are reports elaborating on the effect of LNPs on NLRP3 inflammasomes and toll-like receptors-2/4 (TLR-2/ TLR-4) when the LNPs were modified for their chemical structure and surface charge[39–42]. These studies indicate the inflammatory nature of lipidic carriers and hence, the challenges associated with utilizing conventional LNPs that could be inflammatory and counterproductive for effective inflammasome inhibition and the delivery of inflammasome inhibitors. Moreover, dendritic cells and macrophages (Langerhans cells) are distinguished majorly based on their function. The dendritic cells are a major key player in the activation of adaptive immunity by presenting PAMP/DAMP to the T cells. On the contrary, macrophages are phagocytic cells. Therefore, the LNPs would be first phagocytosed by the macrophages. Inhibiting the inflammasomes in macrophages residing within psoriatic skin using LNPs would convert the pro-inflammatory phenotype (M1) into anti-inflammatory (M2) macrophages thereby, inhibiting chemokine and cytokine release, and other immune cells, which would serve as a negative feedback signal[43].

In this work, we rationalize that developing nanoparticles loaded with inflammasome inhibitors could lead to efficacious inhibition and alleviate psoriasis symptoms. We aimed to design LNPs with self-inflammasome-inhibiting lipids and loaded with inflammasome inhibitors for synergistic inflammasome attenuation in macrophages. Inspired by the recent finding that non-spherical pathogens elicit enhanced adherence to macrophages[44,45], we engineer non-spherical (nanorods and nanoellipses) and spherical LNPs using inflammasome inhibitory lipids (trojan horse) (Fig. 1a) and studied their inflammasome inhibitory efficacy in macrophages. The study involves the development of non-spherical LNP with different shapes (nanospheres/ellipses/rods) to evaluate the impact of shapes on enhanced skin penetration, macrophage adherence, recognition, specificity, and their efficacy in inhibiting inflammasome. To understand their mechanism of action, we elucidate various internalization pathways of the non-spherical LNPs in macrophages (Fig. 1b) and their effect on cellular targets, thereby inhibiting inflammasomes (Fig. 1b). The nanoellipses/rods internalize by macropinocytosis and clathrin-mediated endocytosis, while the nanospheres are majorly phagocytosed. The receptors involved in cellular internalization vary based on the shape of the non-spherical LNP. Moreover, the inhibition of the NLRP3 inflammasomes is significantly higher in macrophages treated with nanorods compared with nanoellipses and nanospheres. Therefore, nanorods are further utilized to develop an efficacious NLRP3-inhibiting anti-psoriatic drug delivery platform.

To overcome the challenges associated with systemic side effects, the present work involves the development of a sprayable polymeric scaffold loaded with lipid nanorods for localized delivery with enhanced skin penetration. Moreover, we aim to achieve a synergistic effect by incorporating an NLRP3 and AIM2 dual inhibitor (NLRP3/AIM2-IN-3; NA3) in NLRP3 inflammasome inhibiting lipid nanorods, delivered topically. Poloxamer-407 (thermogelling agent) and mucin (thickening agent) are utilized to develop a topical spray (Fig. 1c). Mucin was shown to downregulate TLR-4 receptors and inhibit NLRP3 inflammasomes as per previous reports[46]. Here, we demonstrate the synergy of NA3, trojan-horse nanorods, and mucin, which causes dual NLRP3- and AIM2-inflammasome inhibition in the Imiquimod (IMQ)-induced psoriasis-like mice model (Fig. 1d). The NA3-loaded nanorods delay lysosomal rupture, and elicits NLRP3 and AIM2 inflammasome inhibition with reduced ASC speck formation. Interestingly, the sprayable NA3 nanorod-loaded polymeric scaffolds elicit an anti-psoriatic effect by localized reduction of CXCL2, NLRP3-, AIM2 inflammasome, IL-1β, Caspase-1, Gasdermin-D, TLR-7, and TLR-8 RNA levels along with IL-17A protein expression level in-vivo in IMQ-induced psoriasis-like mice model. In summary, the sprayable NA3 nanorod-loaded polymeric scaffold serves as a unique yet simple platform for localized anti-psoriatic delivery, elicits synergy by targeting NLRP3 and AIM2 dual inhibition, and avoids harmful systemic effects.

## Results and discussion

### Synthesis and characterization of nano-spheres/ellipses/rods

It is established that PRR, including but not limited to TLR-4 and a cluster of differentiation 14 (CD14), recognize PAMP and stimulate NLRP3 inflammasome activation[47]. The pathogens are differently shaped, including spherical and ellipsoidal cocci or rod- and spiral or flagellated bacilli[48]. The rod-shaped pathogens cling to the macrophage surface and enhance internalization compared to spherical

https://doi.org/10.1038/s41467-024-53396-x

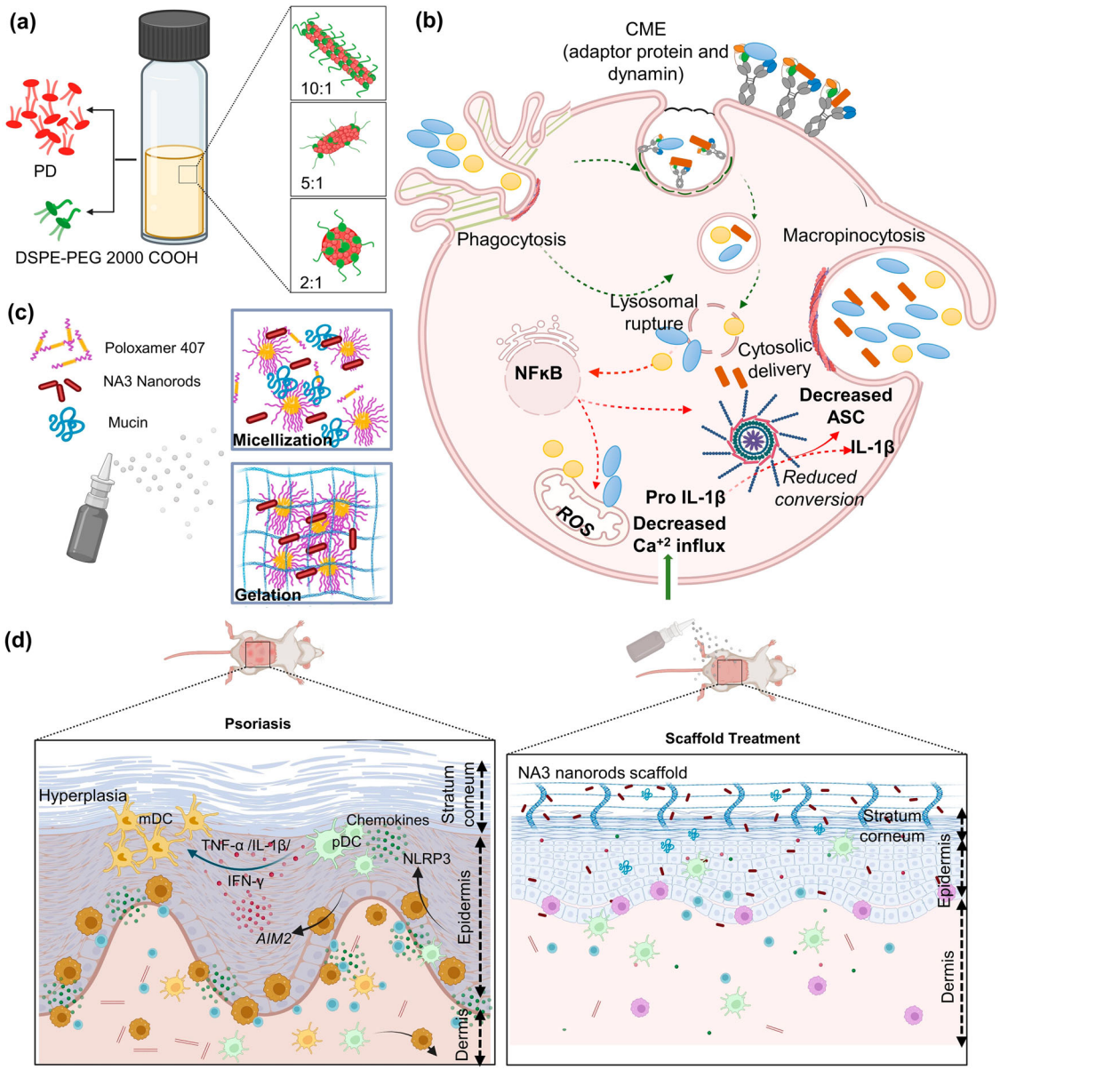


**Fig. 1 | Design and engineering of sprayable polymeric scaffold loaded with non-spherical pathogen-like trojan-horse lipid nanoparticles. a** *Schematic for the synthesis of non-spherical pathogen-like trojan-horse lipid nanorods.* The nanorods, nanoellipses, and nanospheres were prepared using 10:1, 5:1, and 2:1 molar ratios of pyridoxine dipalmitate and DSPE PEG 2000 (carboxylic acid). *Created in BioRender. Kulkarni, A. (2024) BioRender.com/e03e101* **b** *Mechanism of non-spherical lipid nanoparticle cellular internalization and NLRP3 inflammasome inhibition.* The non-spherical lipid nanoellipses/rods were internalized by macropinocytosis and clathrin-mediated endocytosis, while the nanospheres were internalized by phagocytosis. The nanorods delayed lysosomal rupture and significantly reduced the IL-1β level by attenuating ASC speck formation, restraining calcium influx, mitochondrial ROS and NLRP3 inflammasome, whereas the nanoellipses and nanospheres reduced the mitochondrial ROS formation. Created in BioRender. Kulkarni, A. (2024) BioRender.com/q44z068. **c** *Scaffold design and synthesis.* The NLRP3/AIM2-IN-3 (NA3) was loaded within the nanorods, and later, Poloxamer 407 (10% w/v; thermogelling agent) and mucin (2.5 mg/mL; thickening agent) were dissolved in the NA3 nanorods aqueous dispersion to form a solution for topical spraying. When sprayed, the poloxamer solution forms micelles and depicts temperature-dependent gelling properties. Created in BioRender. Kulkarni, A. (2024) BioRender.com/i72q105. **d** In vivo *effect of sprayable polymeric scaffold loaded with nanorods or NA3 nanorods on psoriasis.* The NA3 nanorod polymeric scaffold, when sprayed, causes a thin film due to gelation. The NA3 nanorods and mucin reduce inflammation, psoriatic chemokines, and keratinocyte proliferation due to their effect on NLRP3 and AIM2 inflammasome inhibition. Created in BioRender. Kulkarni, A. (2023) BioRender.com/f54e160.

pathogens[44]. We hypothesized that the shape of the pathogens could be recognized and reminisced by the macrophage receptors and the internalization pathway would differ for non-spherical pathogens compared to spherical ones. Therefore, our objective involved developing pathogen-mimicking lipid-based nano-spheres, ellipses, and rods to study their effect on macrophage targeting, internalization pathway, and inflammasomes inhibition (Fig. 1a, b). Activated inflammasomes are implicated in psoriasis pathogenesis and progression[49]. Pyridoxine (Vitamin B6) is a well-known inflammasome inhibitor and can be utilized as a part of a lipid such as pyridoxine dipalmitate (PD) to facilitate the self-assembly to lipid nanoparticles[50]. Nanorods encompassing PD were developed and transformed into a topical anti-inflammatory formulation eliciting enhanced internalization and targeted delivery to macrophages. We rationalized that the nanorods containing PD would result in trojan-horse pathogen-like LNPs and elicit an anti-inflammatory response.

https://doi.org/10.1038/s41467-024-53396-x

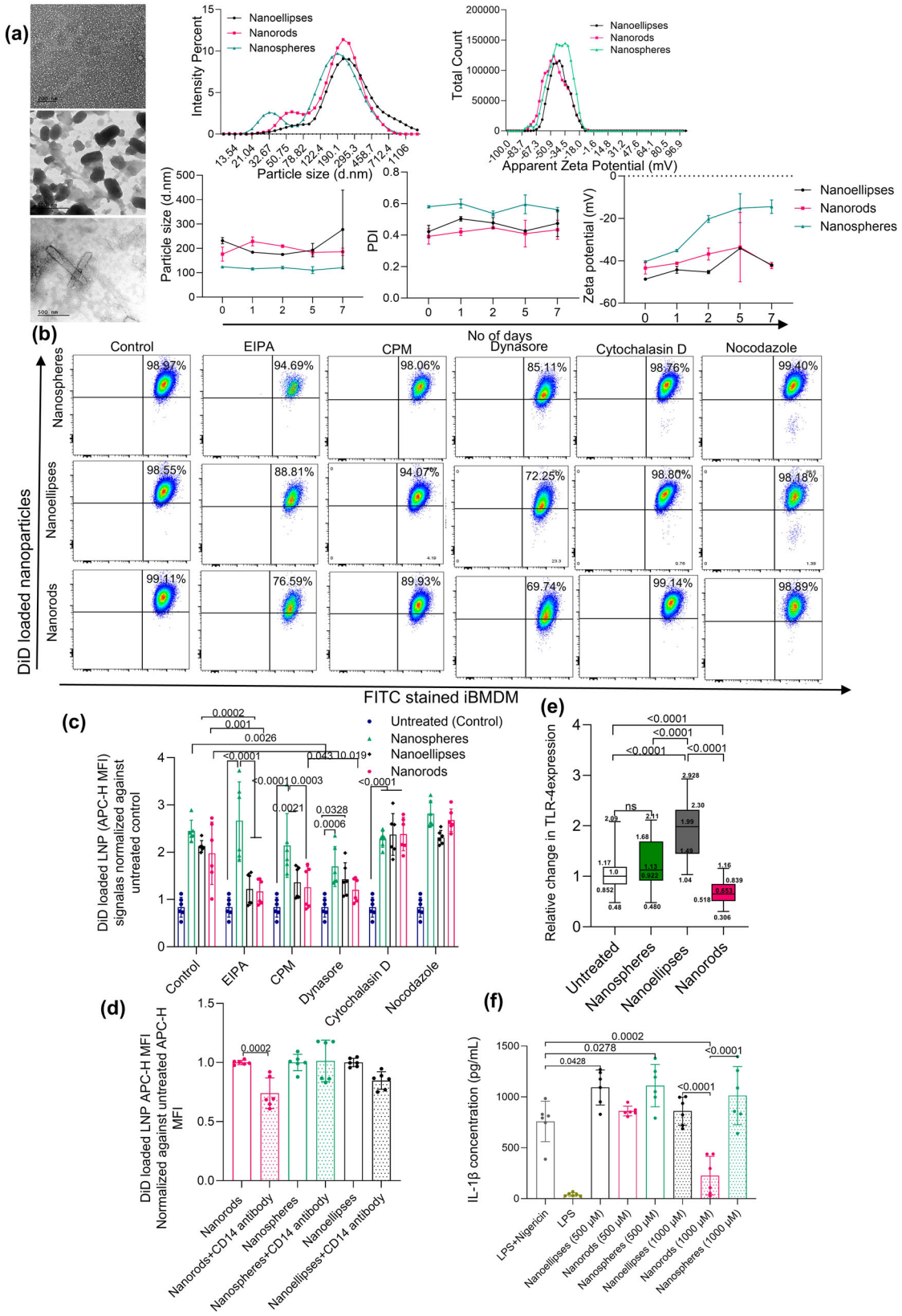


Self-assembled nanoparticles with increasing aspect ratio from spheres to ellipses and rods were developed by using anti-inflammatory PD and DSPE-PEG (2000) carboxylic acid as a stabilizing phospholipid to study the effect of nanoparticle shape on inflammasomes[50,51]. Upon increasing the molar ratio of PD: DSPE-PEG (2000) carboxylic acid from 2:1 to 5:1 and 10:1 increased the aspect ratio of the nanoparticle leading to the formation of nanospheres (124.70 ± 0.43 nm), nanoellipses (231.85 ± 12.37 nm), and nanorods (176.6 ± 28.443 nm), respectively (Fig. 2a). As per the previous report we hypothesize that the increased hydrophobicity of the core and lower curvature of PD in the case of nanoellipses and nanorods, along with the repulsive forces of the PEG chain, led to an increase in the

**Fig. 2 | Evaluation of lipid nanoparticle shape on internalization and inflammasome inhibition in macrophages. a** Synthesis and physicochemical characterization of non-spherical pathogen-like Trojan-horse lipid nanoparticles including Transmission electron microscopy, Particle size, and zeta potential distribution, and stability studies at 4 °C (Data represented as mean ± SD; $n = 3$ individual trials for particle size and zeta potential determination and $n = 2$ for stability studies). **b**, **c** Mechanism of internalization of nano-spheres/ellipses/rods using flow cytometer (Mean ± SD; $n = 6$, 3 biological and 2-technical replicates; data analyzed by two-way ANOVA and Tukey's multiple comparison test). **d**, **e** Internalization of nano-spheres/ellipses/rods through CD14 and TLR-4 determined by flow cytometry and RT-PCR, respectively (Mean ± SD and mean ± SEM, respectively $n = 6$ with 3 biological replicates and 2 technical replicates were used for both the studies, data analyzed by ordinary one-way ANOVA Tukey's multiple comparisons and Brown Forsythe Welche Dunnet's T3 multiple comparisons, respectively. The Fig. 2(e) represents the minima and maxima as the whisker bounds, the 25th and 75th percentile as the bounds of boxes, and the median as the center). **f** Effect of nano-spheres/ellipses/rods on NLRP3 inflammasomes in iBMDM determined by IL-1β ELISA. (Mean ± SD; $n = 6$ with 3 biological replicate and two technical replicate per biological sample data analyzed by ordinary one-way ANOVA and Tukey's multiple comparison test).

aspect ratio of the nanoparticle to form nanoellipses and nanorods[52]. The non-spherical morphology of the LNPs would have reduced Gibb's free energy and enhanced the thermodynamic stability of the system[53,54]. A similar effect was observed previously when the molar ratio of ascorbyl dipalmitate increased the aspect ratio of the nanoparticles to reduce the Gibbs free energy of mixing[52,55,56]. Interestingly, bimodal particle size distribution was observed for nanospheres compared with unimodal particle size distribution for nanoellipses and nanorods (Fig. 2a). The bimodal distribution of nanospheres correlated with previous reports when ascorbyl dipalmitate and DSPE-PEG 2000 were used in 0.125:1 molar ratio[52]. The particle size distribution graph corroborated with the polydispersity index (PDI). The PDI decreased with an increase in the nanoparticle aspect ratio from nanospheres (0.5805 ± 0.006) compared with nanoellipses (0.422 ± 0.039) and nanorods (0.392 ± 0.048), respectively. Furthermore, the particle size and PDI of the nanospheres, nanoellipses, and nanorods remained stable for up to 7 days at 4 °C (Fig. 2a). On the contrary, the zeta potential of the nanospheres increased 2-fold on day 1 and remained stable until day 7. The zeta potential for nanoellipses and nanorods remained consistent until day 7.

## Evaluation of cellular internalization pathway of nano-spheres/ellipses/rods

DiD-loaded nano-spheres/ ellipses/rods were developed to unveil the nanoparticle shape-memory effect of PRR and the mechanism of cellular internalization in immortal bone marrow-derived macrophages (iBMDMs). PD, DSPE-PEG 2000 carboxylic acid, and DiD (0.067% w/w) were dissolved in dichloromethane (DCM) and evaporated to form a thin film. The thin film was rehydrated using Milli-Q to form the DiD-loaded nano-spheres/ellipses/rods. The DiD-loaded nano-spheres/ellipses/ rods were internalized efficiently by the iBMDMs (Fig. 2b, c). Apart from phagocytosis, various internalization pathways exist in iBMDM cells, including macropinocytosis, caveolae-, and clathrin-mediated endocytosis[57]. The mean fluorescence intensity of DiD-loaded nano-spheres, ellipses, and rods was measured in iBMDM pretreated with macropinocytosis, phagocytosis, clathrin-(CME), dynamin-dependent endocytosis inhibitors to elucidate the cellular internalization pathway. It was observed that the internalization decreased with an increase in an aspect ratio of nanoparticles from spheres to ellipses and rods in iBMDMs pretreated with EIPA, CPM, and Dynasore inhibiting macropinocytosis, CME, and dynamin-dependent endocytosis, respectively. The cellular uptake of DiD nanoellipses was 3.2-, 1.9-, and 1.6-fold lower compared with nanospheres in iBMDMs pretreated with EIPA, CPM, and Dynasore (Fig. 2b, c). Whereas the DiD-loaded nanorods depicted reduced internalization by 3.2-, 2.3-, and 2.03-folds compared with nanospheres in iBMDMs pretreated with EIPA, CPM, and Dynasore, respectively (Fig. 2b, c). On the contrary, the cellular uptake was unaffected by the pre-treatment of cytochalasin D (actin polymerization inhibitor affecting phagocytosis) and Nocodazole (microtubule and spindle formation inhibitor) (Fig. 2c) These results demonstrated that the nanoellipses and nanorods were internalized primarily by macropinocytosis and clathrin-mediated endocytosis in iBMDMs due to their significant reduction in internalization in the presence of EIPA ($p < 0.0001$) and CPM ($p < 0.001$ and 0.01), respectively. In contrast, the nanospheres were internalized majorly by phagocytosis due to their reduced internalization in iBMDMs pretreated with Dynasore. The clathrin pits endocytose the receptors; therefore, the non-spherical LNPs would be recognized through specific receptors before endocytosis through clathrin pits.

CD14 protein is instrumental in recognizing damage-associated molecular protein (DAMP) and pathogen-associated molecular protein (PAMP), activating canonical and non-canonical inflammasome pathways[58]. The literature revealed that lipopolysaccharide (LPS; PAMP) is recognized by both CD14 and TLR-4, while oxidized phosphorylcholine (ox-PAPC) derivatives (DAMP) are recognized only by CD14 without the involvement of TLR-4 activating the NLRP3 inflammasome[59]. Therefore, the involvement of the CD14 and TLR-4 in the internalizaition of nano-spheres/ellipses/rods was further explored. The CD14 receptor was blocked using anti-CD14 fluorescein isothiocyanate (FITC) antibody. The FITC signals increased significantly in anti-CD14 antibody treated iBMDMs (Supplementary Fig. 1a). Interestingly, the internalization of nanorods was significantly reduced by 1.36-and 1.2-fold compared with nano-spheres ($p < 0.0001$) and nanoellipses, respectively when the CD14 receptors were blocked using anti-CD14 FITC antibody. Moreover, the internalization of nanorods was decreased significantly ($p < 0.001$) compared with iBMDMs without CD14 FITC antibody treated group (Fig. 2d). Therefore, the CD14 receptors could exclusively recognize the non-spherical nanorods compared with nano-spheres and nanoellipses. Furthermore, it was observed that the relative expression of TLR-4 increased in iBMDMs treated with nanoellipses compared with nanorods ($p < 0.0001$) (Fig. 2e). These results demonstrated that the nanoellipses were internalized through CD14 and TLR-4, whereas the internalization of nanorods occurred only through the CD14 receptor. In comparison, the expression of CD14 and TLR-4 remained unaffected in iBMDMs treated with nanospheres, which were primarily phagocytosed.

## Cytotoxicity studies of nano-spheres/ellipses/rods by MTT assay

The cellular IL-1β inflammatory cytokine levels largely depend upon cellular viability. IL-1β binds to IL-1 receptors on the surface of immune cells and triggers further inflammatory processes[60]. However, prolonged NLRP3 inflammasome activation expedites pyroptosis, which might diminish IL-1β levels[61]. The Trojan-horse nanoparticles were anticipated to elicit an inhibitory effect on NLRP3 inflammasomes without causing cytotoxicity. The cytotoxic effect of the nanospheres, ellipses, and rods in iBMDMs was determined by MTT assay. Combined activation by LPS (signal 1) and Nigericin (Signal 2) caused pyroptosis with 45.86 ± 7.2% iBMDM cell viability. On the contrary, the cell viability was significantly higher ($p < 0.0001$) in iBMDMs treated with LPS (90.07 ± 19.12%), and 500 μM or 1000 μM of nano-spheres (94.0 ± 13% and 100 ± 20%), ellipses (95.0 ± 10% and 94.64 ± 11.6%), and rods (87.15 ± 11.8% and 92.03 ± 11.9%) compared with LPS and Nigericin treated iBMDMs (Supplementary Fig. 1b). Therefore, the nano-spheres, ellipses, and rods at 500 μM and 1000 μM concentration levels were considered safe for iBMDMs.

### Effect of nano-spheres/ ellipses/ rods on in-vitro NLRP3 inflammasome inhibition

The inhibitory effect of the nanoparticles on NLRP3 inflammasomes in the LPS and Nigericin (positive control)[62] activated iBMDMs would be evident with reduced IL-1β levels. It was observed that nanospheres and nanoellipses (500 μM and 1000 μM) did not inhibit the inflammasome activation in Nigericin-treated iBMDMs (Fig. 2f). Moreover, the inhibitory effect of the nanorods diminished in iBMDMs activated with LPS (Supplementary Fig. 1c). The LPS is known to bind the TLR4 along with co-receptor CD14 and furnishes signal 1 for NLRP3 inflammasome activation[47]. It was reported that oxidized phospholipid 1-palmitoyl-2-arachidonoyl-sn-glycero-3-phosphorylcholine (ox-PAPC, cellular DAMP) utilizes CD14 to internalize within the cells and activate NLRP3 inflammasomes[59]. Therefore, we hypothesize based on the nanorods' cellular internalization mechanism involving LPS recognizing CD14 receptor protein (Fig. 2d) that the nanorods might mimic the ox-PAPC as trojan horse and successfully inhibit NLRP3 inflammasomes.

Significant concentration-dependent NLRP3 inflammasome inhibition was observed when iBMDM was treated with nanorods followed by LPS. Also, 1.3-fold (500 μM) and 3.8-fold (1000 μM) NLRP3 inflammasome attenuation was observed in nanorods pretreated iBMDM compared with nanoellipses (Fig. 2f). To conclude, the aspect ratio of the trojan-horse nanoparticles was directly proportional to the extent of NLRP3 inflammasome inhibition in iBMDMs. Moreover, upregulation of TLR-4 RNA expression in nanoellipse-treated iBMDMs, as observed previously (Fig. 2e), would have resulted in lower NLRP3 inflammasome inhibition than nanorod-treated iBMDMs. Additionally, Pyridoxine elicits an antioxidant and anti-inflammatory effect. Therefore, the reduced IL-1β level caused by the trojan-horse nanorods could be attributed to higher PD compared with nano-spheres and ellipses[50]. These results elucidate further the various mechanisms resulting in the inhibitory effect on NLRP3 inflammasomes. Based on the recent report, we hypothesize greater adherence of the nanorods onto the macrophage, which might diminish protracted LPS-induced signal 1 stimulation required for activation of NLRP3 inflammasome[63,64].

### Effect of nano-spheres/ellipses/ rods on ASC speck and lysosome

The NLRP3 inflammasome is a multi-protein complex that when activated causes oligomerization of adaptor-protein apoptosis-associated speck-like protein containing pyrin domain (ASC), and causes caspase activation and recruiting domain (CARD)[65]. The ASC further oligomerizes and activates pro-caspase-1, which upon auto-proteolysis cleaves to caspase-1. Caspase-1 stimulates the release of cytokines, gasdermin D pore formation, and pyroptosis[61]. After that, the released ASC and caspase-1 further activate the NLRP3 inflammasomes in other cells (Fig. 3a)[66]. Given the significance of ASC in NLRP3 inflammasome activation, an orthogonal technique of determining the ASC speck formation could further confirm the ability of the nano-spheres/ellipses/ rods to inhibit the NLRP3 inflammasomes. The number of ASC specks per live cell was significantly reduced in iBMDMs pretreated with nanoellipses ($p < 0.01$) and nanorods ($p < 0.001$) compared with iBMDMs treated with positive control (Fig. 3b, c). Moreover, no significant difference was observed in the iBMDMs treated with nanospheres compared with positive control. The ASC speck per live cell was 3.2- and 11.5-fold higher in iBMDMs treated with nanospheres compared with nanoellipses ($p < 0.001$) and nanorods ($p < 0.0001$), respectively. Therefore, increasing the aspect ratio of the nanoparticles effectively inhibits ASC speck formation required for downstream inflammatory signaling cascade.

The DAMP and nanoparticle associated molecular pattern (NAMP) are internalized and released into the cytosol by lysosomal rupture, triggering the oligomerization of ASC and NLRP3 activation (Fig. 3d)[38,61]. The majority of bacteria[67,68] and viruses[69] endocytose, resulting in lysosomal rupture and cathepsin B release activating NLRP3 inflammasomes[70]. Interestingly, the pathogen-like nanorods depicted reduced lysosomal rupture compared with nanoellipses ($p < 0.05$) and nanospheres ($p < 0.01$) (Fig. 3e–g). Although nanoellipses and nanorods could reduce the ASC speck formation, only nanorods efficiently delayed lysosomal rupture compared with nanoellipses which could cause significant impact on the inhibition of NLRP3 inflammasomes. Moreover, Nigericin is a well-known signal 2 that activates inflammasome without lysosomal rupture by increasing potassium efflux[71]. Therefore, significantly higher intact lysosomes were observed in LPS and Nigericin-treated iBMDMs (Fig. 3g). Evasion of lysosomal rupture through membrane-bound blebs by macropinocytosis is one of the primary mechanisms for virus entry[72]. We hypothesize that the inhibition of lysosomal rupture observed in the case of nano-ellipses and rods compared with nanospheres could be attributed to their internalization through macropinocytosis (similar to the mechanism of virus entry) in addition to Clathrin-mediated endocytosis (Fig. 3d, Fig. 2c) as trojan horses.

### Effect of nano-spheres/ellipses/ rods on Calcium influx and mitochondrial reactive oxygen species

Under ordinary conditions, the cytosolic calcium is significantly lower than the extracellular (<200,000-folds) and endoplasmic reticulum or lysosome (<5000-folds)[73]. However, the membrane depolarization and endoplasmic reticulum/lysosomal membrane permeabilization cause a continuous inflow of calcium due to an electrochemical gradient[74]. Since the developed trojan horse LNPs caused lysosomal membrane permeabilization, observing the effect on calcium influx would be noteworthy. It was observed that Nano-spheres, ellipses, and rods restrained the intracellular calcium in iBMDM cells similar to the LPS and Nigericin (positive control) treated iBMDMs. Potassium efflux is associated with calcium influx through the cell membrane channel[75]. Nigericin is a known NLRP3 signal 2 molecule that increases potassium efflux through the cellular membrane, resulting in calcium influx upstream of NLRP3 inflammasomes. Therefore, the increase in calcium influx for Nano-spheres/ellipses/rods could be attributed to the combined effect of Nigericin-induced calcium influx through the cell membrane and the release of lysosomal calcium stores. (Fig. 3h).

Identification of DAMP, NAMP, or PAMP is associated with various cellular responses, including increased cell volume, membrane permeabilization, and mitochondrial ROS (mtROS) generation[76]. Therefore, the effect of nano-spheres, ellipses, and rods was evaluated for their efficacy against mtROS generation. The nanospheres ($p < 0.001$), nanoellipses ($p < 0.001$ and 0.0001), and nanorods ($p < 0.0001$ and 0.01) were effective in inhibiting the mtROS generation in iBMDMs by 2.3–3.9-folds when compared with positive control (Fig. 3i). Each group treated with the nano-spheres/ellipses/rods were activated by LPS (signal 1) and Nigericin (signal 2) and the efficacy of the nanospheres/ellipses/rods to attenuate mtROS was determined. Nigericin elicits an effect on mtROS generation through NLRP3-dependent and stress-induced severe mitochondrial dysfunction (NLRP3 independent pathway)[77]. However, the current study aimed to elucidate whether the effect of nano-spheres/ellipses/rods on mtROS generation was caused due to activated NLRP3 inflammasomes.

An increase in lysosomal membrane permeabilization leads to calcium efflux, signaling the endoplasmic reticulum and mitochondrion. This leads to the generation of mtROS production. However, PD is an antioxidant that could inhibit the ROS[50,78]. Therefore, the increased mtROS inhibition observed in the case of nano-ellipses and spheres could be attributed to higher lysosomal rupture in iBMDMs treated with nano-ellipses and spheres, causing enhanced cytosolic PD concentration and mtROS inhibition. Whereas, the nanorods were efficacious compared with nano-spheres and ellipses in NLRP3 inflammasome attenuation due to decrease in TLR-4 upregulation, ASC speck formation, NLRP3 oligomerization, mtROS formation, and lysosomal rupture.

https://doi.org/10.1038/s41467-024-53396-x

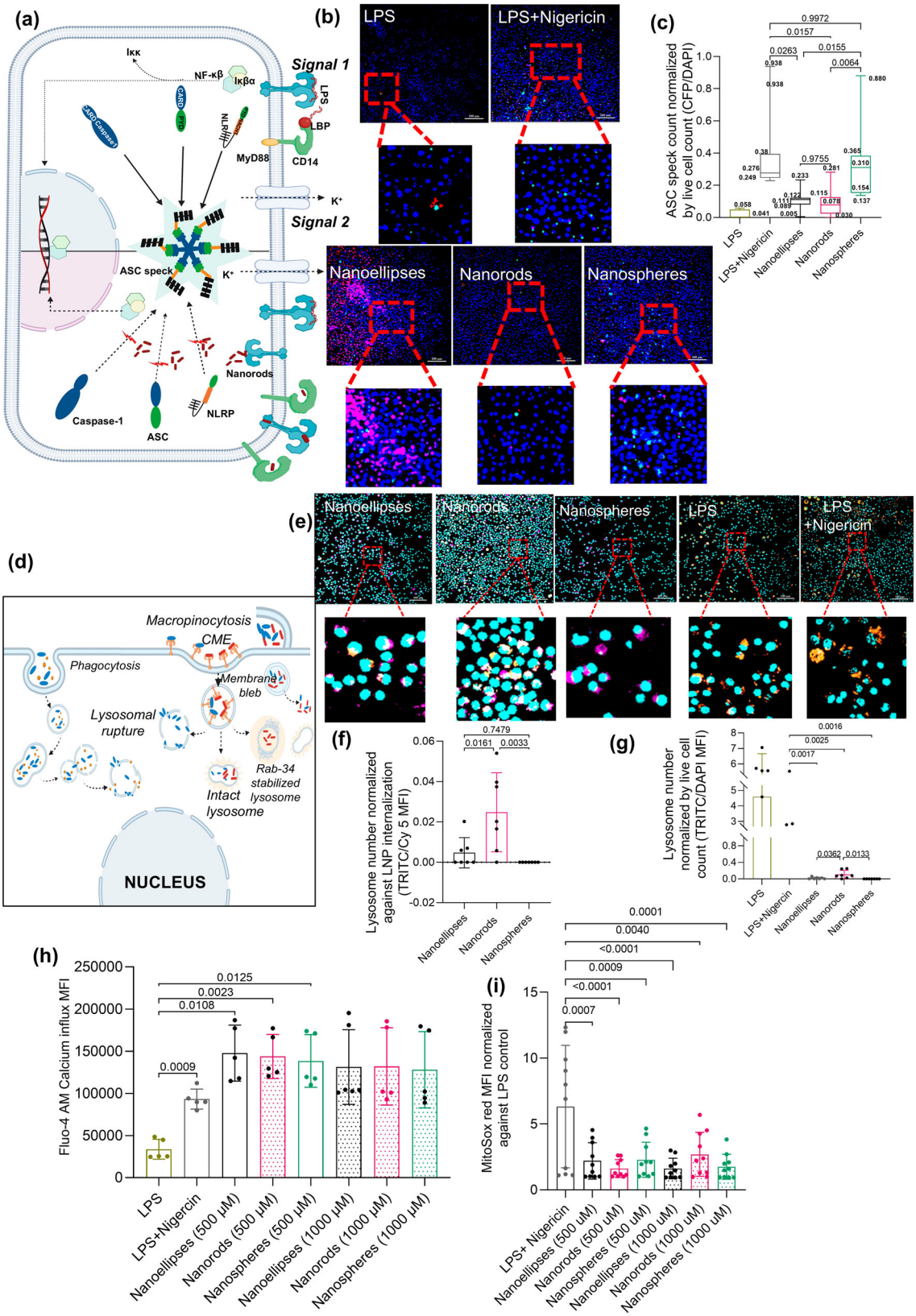


## NA3 nanorod-loaded scaffold design and characterization

Exacerbated keratinocyte proliferation and psoriatic lesions are caused by the combination of NLRP3 and AIM2 inflammasomes[5,79]. Administration of immunosuppressants would enhance the risk of comorbidities in the case of psoriasis[80]. Therefore, localized simultaneous modulation of NLRP3 and AIM2 inflammasomes in macrophages of psoriatic skin coax safe recovery from psoriasis. The NA3 was loaded into the nanorods to enhance the efficacy toward both NLRP3 and AIM2 (Fig. 4a). The critical process parameters, including sonication time and lipid concentrations, were optimized to yield stable NA3 nanorods (234.6 ± 4.7 nm, 0.42 ± 0.02, −43.3 ± 1.3 mV) (Fig. 4b, c). The NA3 nanorods were stable for 7 days at 4 °C (Fig. 4d)

https://doi.org/10.1038/s41467-024-53396-x

**Fig. 3 | Mechanistic evaluation of lipid nanoparticles (LNPs) shape on inflammasome inhibition in macrophages. a** Schematic representation of the effect of LNP shapes on ASC speck formation. Created in BioRender. Kulkarni, A. (2023) BioRender.com/i04d511. **b** Confocal microscopic images of ASC speck (CFP) in iBMDM with nano-spheres/ellipses/rods at 20X (Scale bar: 100 μm). **c** ASC speck number per cell when treated with nano-spheres/ellipses/rods. (Mean ± SD, $n = 3$ biological replicates with 4 technical replicates per biological sample using Brown Forsythe Welche one-way ANOVA and Dunnett's T3 multiple comparison. The graph represents the minima and maxima as the whisker bounds, the 25th and 75th percentile as the bounds of boxes, and the median as the center) (**d**) Schematic representation of the effect of LNP shapes on lysosomal rupture. Created in BioRender. Kulkarni, A. (2023) BioRender.com/l77q945. **e** Confocal microscopic images of intact lysosomes (TRITC) in iBMDM treated with nano-spheres/ellipses/rods at 20X (Scale bar: 100 μm). **f**, **g** Analysis of intact lysosomes normalized against LNP internalization and live cells as indicated by Cy5 and DAPI signal, respectively when treated with nano-spheres/ellipses/rods. Each data represented as mean ± SD; $n = 7$; with 3 biological replicate and 2,2,3 technical replicates data analyzed by ordinary one-way ANOVA and Tukey's multiple comparisons. **h**, **i** Effect of nano-spheres/ellipses/rods on calcium influx and mitochondrial ROS formation determined by flow cytometer. (Each data represented as mean ± SD; $n = 5$ with 2 biological and 2, 3 technical replicates and $n = 10$; with 4 biological and 2,2,3,3 technical replicates, data analyzed by Brown Forsythe Welche one-way ANOVA with Dunnets T3 multiple comparison and ordinary one-way ANOVA, respectively).

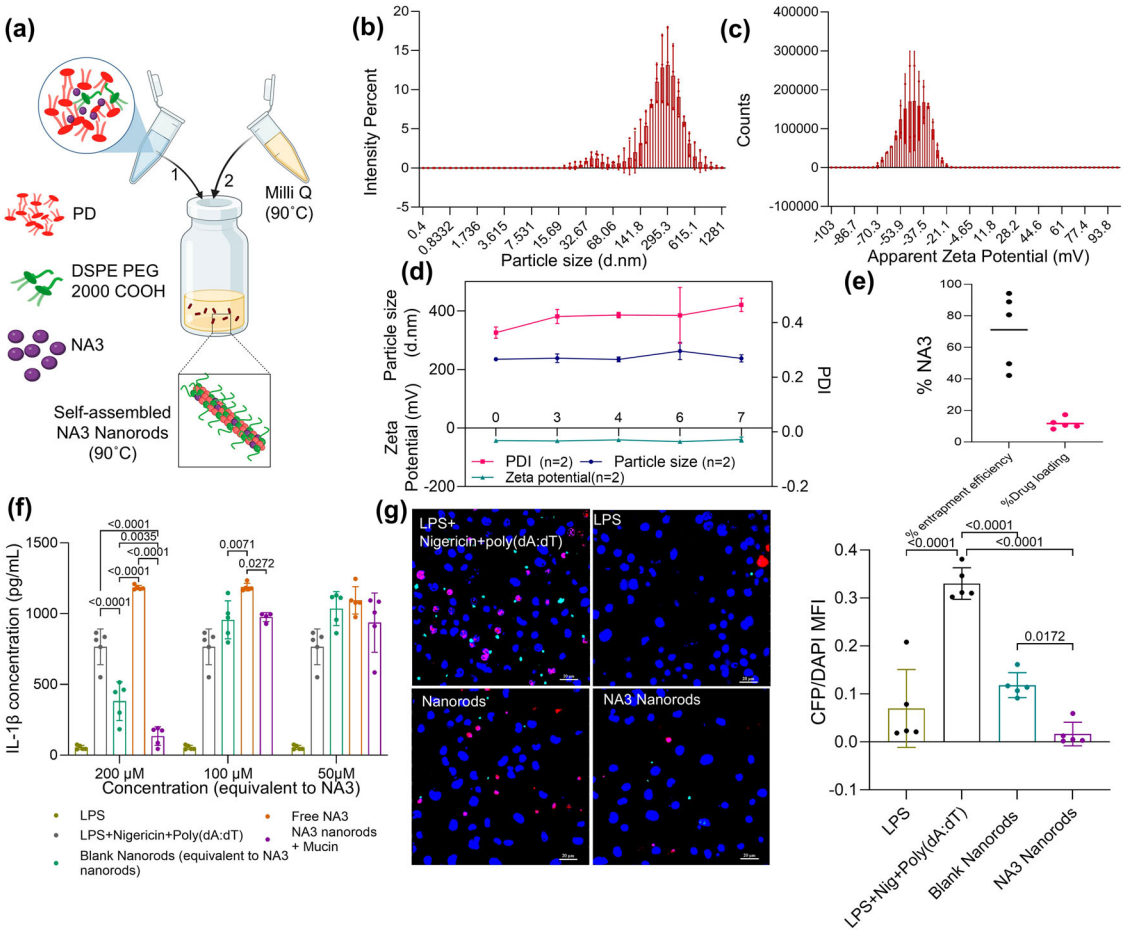


**Fig. 4 | Effect of NLRP3-AIM2 inhibitor (NA3) loaded nanorods on inflammasome inhibition. a** Schematic of NA3 nanorods synthesis. Created in BioRender. Kulkarni, A. (2023) BioRender.com/o21z452. **b**, **c** Particle size (mean ± SD; $n = 3$ individual trials) and zeta potential distribution (mean ± SD; $n = 2$ individual trial) of NA3 loaded nanorods (**d**) Time-dependent stability studies of NA3 nanorods at 4 °C (Data represented as mean ± SD; $n = 2$ individual trials). **e** % drug loading and % encapsulation efficiency of NA3 in nanorods determined by RP-HPLC ($n = 5$ individual replicates). **f** Effect of NA3 loaded nanorods on inflammasome inhibition in iBMDM determined by IL-1β ELISA (Each data represented as mean ± SD; $n = 5$ with 2 biological replicate and 2,3 technical replicate per biological replicate; data analyzed by two-way ANOVA with Tukey's multiple comparisons). **g** Effect of NA3 nanorods on ASC speck formation determined by confocal microscopy (Each data represented as mean ± SD; $n = 5$ with 2 biological replicate and 2 and 3 technical replicate per biological replicate data analyzed by ordinary one-way ANOVA and Tukey's multiple comparison). The images were observed at 60X (scale bar 20 μm).

with the NA3 loading and % entrapment efficiency of 11.70% ± 3.5% and 71.11% ± 23.6%, respectively (Fig. 4e).

One study compared the efficacy of NA3 on NLRP3 and AIM2 inflammasomes in both J774A.1 cells and bone marrow-derived macrophages (BMDMs)[81]. NA3 depicted lower efficacy on AIM2 inflammasomes in J774A.1 cells compared with BMDMs while the drug elicited significantly higher efficacy on NLRP3 inflammasomes in J774A.1 cells ($IC_{50}$-19.62 μM) compared with BMDMs ($IC_{50}$-48.98 μM)[81]. However, in presence of the Poly dA:dT (AIM2 stimulating signal 2) the NA3 loaded nanorods elicited enhanced efficacy ($p < 0.0001$) against NLRP3 and AIM2 inflammasomes in iBMDMs compared with free NA3 and blank nanorods. It was observed that the in-vitro efficacy of the NA3 loaded nanorods (equivalent to 200 μM NA3) depicted 21.5- and 59-fold reduction in IL-1β levels compared with blank nanorods and free NA3, respectively (Fig. 4f). Therefore, the efficacy of NA3 was improved compared with free NA3 when incorporate within nanorods. Since the activation of both NLRP3 and AIM2 results in ASC speck formation, we further studied the effect of NA3-loaded nanorods on ASC speck. The

https://doi.org/10.1038/s41467-024-53396-x

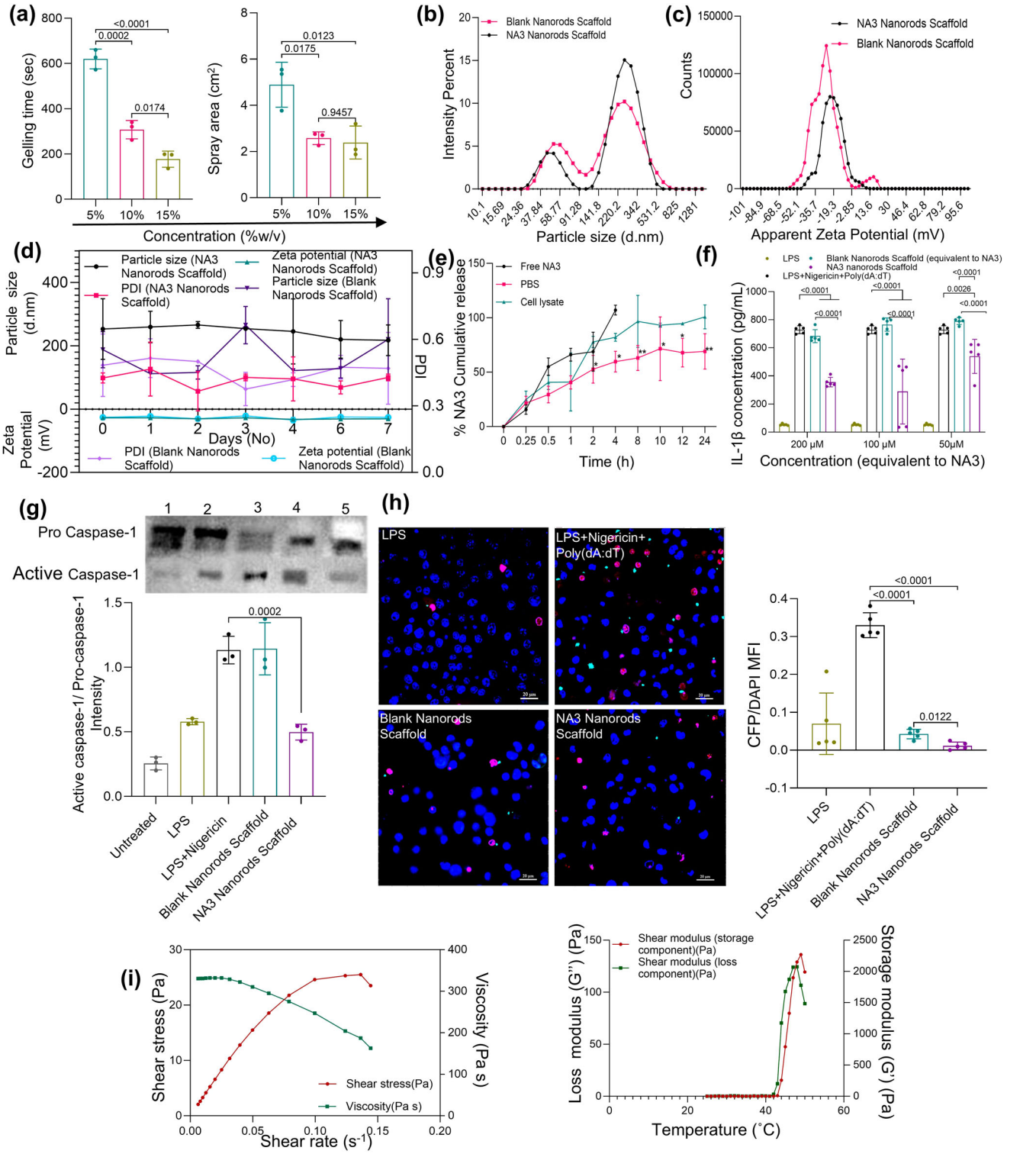


results corroborated with the IL-1β ELISA with an 11.9-fold reduction in ASC speck formation compared with blank nanorods (Fig. 4g).

To facilitate the topical application of NA3-loaded nanorods, a thermogelling excipient was essential. Poloxamer 407, due to the presence of poly(propylene oxide)(PPO) and poly(ethylene oxide) (PEO) groups, elicits micellization and gelation at 37 °C and ensures low toxicity due to its non-ionic nature[82,83]. It is reported that Poloxamer 407 was used in topical formulations with upto 20% w/v concentration[84]. It was observed that the gelling time decreased from 620 s ± 43.9 s to 177.3 s ± 35.8 s with increased Poloxamer 407 concentration (5%–15 w/v) (Fig. 5a). Similarly, the spray area of 5% w/v poloxamer solution was significantly higher (4.8 ± 0.95 $cm^2$)compared with 10% w/v (2.6 ± 0.27 $cm^2$) and 15% w/v (2.4 ± 0.71 $cm^2$) ($p < 0.05$) (Fig. 5a). Considering the required consistency, a sprayable NA3-loaded scaffold containing 10% w/v Poloxamer 407 was utilized for topical administration. Mucin (2.5 mg/mL) was used as a thickening agent to enhance the viscosity further and improve the anti-inflammatory effect (Fig. 1c). We hypothesized that the non-ionic surfactant property of Poloxamer 407 would enhance the penetration of the NA3 nanorods and hydrophilic mucin (Fig. 1c,d) within the

**Fig. 5 | Effect of NLRP3-AIM-2 inhibitor (NA3) loaded nanorods polymeric scaffold on inflammasome inhibition. a** Screening of thermogelling polymer concentration (Data represents mean ± SD, $n = 3$ individual experiments analyzed by one-way ANOVA and Tukey's multiple comparison test) (**b**, **c**) Particle size and zeta potential distribution, respectively of NA3 loaded nanorods polymeric scaffold. **d** Time-dependent stability studies of NA3 nanorods polymeric scaffold at 4 °C (Mean ± S.D; $n = 2$ individual formulations). **e** In-vitro drug release of NA3 from NA3-loaded nanorods polymeric scaffold in PBS and cell lysate. (Each data represents mean ± SD; $n = 6$ for NA3 nanorods polymeric scaffold, n = 3 and 2 for NA3 nanorods scaffold drug release in cell lysate and free NA3, respectively. Data analyzed by two-way ANOVA, $p = 0.0182, 0.040, 0.0010, 0.0486, 0.0107, 0.0021$ for NA3 nanorods polymeric scaffold in PBS compared with NA3 nanorods polymeric scaffold in cell lysate) (**f**) Effect of NA3 loaded nanorods polymeric scaffold on inflammasome inhibition in iBMDM determined by IL-1β ELISA. (Each data represents mean ± SD; n = 5 with 2 biological replicate and 2,3 technical replicate and analyzed by two-way ANOVA and Tukey's multiple comparisons). **g** Effect of NA3 loaded nanorods and blank nanorods polymeric scaffold on caspase-1 determined by western blot in iBMDM (1-untreated, 2-LPS (Negative control), 3-LPS+Nigericin (positive control), 4-Blank nanorods polymeric scaffold, 5-NA3 nanorods polymeric scaffold treated iBMDM) (Each data represents mean ± SD; $n = 3$ technical replicate per biological sample and analyzed by one-way ANOVA and Tukey's multiple comparisons). The samples were obtained from same experiment and the blots were run in parallel on the same gel. The uncropped gels are available in the supplementary and source data file. **h** Effect of NA3 nanorods polymeric scaffold on ASC speck formation determined by confocal microscopy. The images were observed at 60X magnification (scale bar-20 μm) (Each data represented as mean ± SD; $n = 5$ with 2 biological and 2,3 technical replicates and analyzed by Brown Forsythe Welche one-way ANOVA with Dunnett's T3 multiple comparison). **i** Rheological studies of NA3 nanorods polymeric scaffold.

thickened psoriatic skin. The NA3 nanorod polymeric scaffold (252.75 ± 95.8 nm, 0.426 ± 0.02, −27.5 ± 0 mV) and the blank nanorods polymeric scaffold (187.7 ± 57.13 nm, 0.48 ± 0.14, −26 ± 3.7 mV) were stable for 7 days at 4°C (Fig. 5b–d). The sprayable NA3 nanorod polymeric scaffold led to sustained NA3 release (69.09 ± 16.27%) up to 24 h in PBS (Fig. 5e). Furthermore, the drug release kinetics of NA3 nanorods polymeric scaffold was done in the presence of cell lysate. The cumulative drug release was found to be 96.67 ± 23.9% within 8 h in cell lysate. Therefore, the NA3 nanorods would lead to quick release once within the macrophages. On the contrary, 107.1 ± 4.5% NA3 was released within 4 h in the case of free drug. The in vitro efficacy of NLRP3 and AIM2 inhibition by sprayable NA3 nanorods polymeric scaffold was evaluated by IL-1β ELISA in iBMDMs. Dual inhibition of NLRP3 and AIM2 inflammasomes in iBMDMs led to significantly lower IL-1β concentration ($p < 0.0001$) compared with blank nanorods scaffold (Fig. 5f). Moreover, the NA3 nanorods scaffold (50–200 μM NA3 equivalent) caused 1.8–2.2 fold reduction in IL-1β levels directly correlating with reduced NLRP3 and AIM2 inflammasome activation compared with blank nanorods. In contrast, only a 1.5-fold reduction in IL-1β level indicating the NLRP3/AIM2 inflammasome reduction was observed in iBMDMs treated with blank nanorods scaffold (equivalent to 200 μM NA3) compared with the positive control ($p < 0.0001$) (Fig. 5f). Earlier, we observed that nanorods caused downregulation of TLR-4 RNA expression, delayed lysosomal rupture, and ASC speck formation. However, their effect on active caspase-1 was not elucidated. The NA3 nanorod polymeric scaffold significantly reduced active caspase-1 formation compared with positive control ($p < 0.001$). On the contrary, the blank nanorods did not have any effect on active caspase-1 (Fig. 5g). Therefore, the NA3 nanorod-loaded polymeric scaffold caused significantly lower IL-1β levels resulting from decreased NLRP3 and AIM2 inflammasome formation compared with the blank nanorod-loaded scaffold due to the inhibition of caspase-1. The NA3 nanorod-loaded and blank nanorod-loaded polymeric scaffolds reduced the ASC speck formation compared with the positive control group ($p < 0.01$). When the number of ASC specks per live cell was analyzed by confocal microscopy, a 2-fold reduction in ASC speck formation was observed in iBMDMs treated with NA3 nanorod-loaded polymeric scaffold compared with blank nanorod-loaded polymeric scaffold (Fig. 5h).

The development of topical spray was instigated to support ease of administration and patient compliance. However, a reversible shear thinning and solid-like behavior is desirable for quick administration through the spray nozzle[85]. Poloxamer 407 aqueous solution is widely used as a fluid that encompasses temperature-dependent yield stress, the ability to reduce viscosity on the application of shear stress, and forms a weak gel when in contact with a surface[84]. Moreover, the anti-fouling effect and anti-protein adsorption make it suitable for topical spray[86]. The viscosity at a sol-gel temperature of Poloxamer 407 was 12.09 and 165 Pa.s at 10% w/v and 15% w/v, respectively (Supplementary Fig. 3a). However, the higher viscosity of the gel reduces the penetration ability of the nanoparticles within the skin when applied topically. For instance, an increase in viscosity of cellulose from 16.3 ± 1.05 Pa.s to 40.4 ± 3.11 Pa.s reduced penetration of Sulphadiazene sodium by 1.66 folds[87]. Therefore, an optimal 10% w/v Poloxamer 407 concentration was used to develop a sprayable scaffold. The mucin provided an additive effect that formed a mesh-like network above 1.875 mg/mL concentration[88]. Hence, we decided to utilize Poloxamer 407 and mucin (as an anti-inflammatory thickening agent) to develop a sprayable scaffold. An increase in shear rate caused decreased viscosity of the sprayable NA3 nanorod polymeric scaffold, eliciting shear thinning behavior when passed through the spray bottle nozzle (Fig. 5i). The NA3 nanorod scaffold showed sol-gel transition at 43 °C with an increase in viscosity from 2.41 Pa.s (43 °C) to 361.4 Pa.s (49 °C). As per the previous reports, the storage/elastic modulus (G') and loss/viscous modulus (G") increased rapidly at the sol-gel transition, eliciting the thermogelling nature of the scaffold (Fig. 5i).

### In-vivo efficacy of sprayable NA3 nanorod-loaded polymeric scaffold in imiquimod (IMQ)-induced psoriasis-like Balb/c mice

As per the literature, the 2D and 3D in-vitro human cell-based models have been developed using human keratinocytes co-cultured with T-cells/macrophages and inflammatory cytokines aggravating keratinocyte proliferation[89,90]. Certain drawbacks with in vitro models include morphological dysfunction of necrosis, spongiosis, and parakeratosis even before losing keratinocyte integrity[91], improper selection of culture media mimicking the fluid volume in the psoriatic skin tissue, dose extrapolation, loss of disease phenotype during cell expansion[90], lack of reproducibility[92] and scarcity of the source of psoriatic lesional skin[90], inability to estimate the vascular inflammation and hypervascularization[90], and inability to predict the systemic effect. On the contrary, the in-vivo model exactly illustrates the involvement of inflammatory mediators, the communication between innate and adaptive immune systems, the role of resident cells, and the evaluation of new therapies[93]. Therefore, we decided to confirm the efficacy of NA3 nanorods and blank nanorod-loaded polymeric scaffold in the mice psoriasis model.

Animal models should be selected based on species that develop similar diseases, augmentation of key molecule or cell type, and/or inhibition of target molecule or cell type[93]. Therefore, the appropriate animal model for the present study should include an aggravated inflammasome response causing chronic psoriasis-like symptoms which is observed in IMQ-induced or IL-23 induced psoriasis like mice model. IMQ stimulates the activation of NLRP3 and AIM2 inflammasomes through TLR 7/8 receptors[94]. Similarly, IL-36 and Keratin-14 (K14) promoters cause psoriasis-like symptoms by activation of NLRP3 inflammasome and IL-17/IL23 axis[95]. However, an IMQ-induced psoriasis-like mice model was used in the current study considering its acceptability, ease of psoriasis induction, and cost[96]. Furthermore,

IMQ-induced psoriasis-like models closely resemble human psoriasis including infiltration of both innate and adaptive immune cells (Th17 and Th22 responsible for IL-17A/IL-23 axis activation), dendritic cells, macrophages, keratinocytes leading to parakeratosis, acanthosis, rete-ridges, and vascular hyperproliferation, and hyperplasia[90]. Therefore, the difference in the efficacy of blank nanorods, NA3 nanorods treated polymeric scaffold versus IMQ-treated and vaseline (positive and negative control) were more pronounced in the IMQ-induced psoriasis-like model.

Furthermore, other in-vivo models are associated with several disadvantages that includes dermal infiltration including mast cells, macrophages, and neutrophils without the involvement of cross-talk between innate and adaptive immune cells (T-cells), no-efficacy against cyclosporin (calcineurin inhibitor) in spontaneous mutation model[93], complexity in identification and modification of genes to establish chronic skin inflammation in genetically modified mice psoriasis model[97], variation in the penetrance of the transferred T-cell phenotypes and prioritizing only T-cells in immune cell induced psoriasis-like model[93], unpredictable phenotype and inappropriately developed skin model representing more like atopic dermatitis than psoriasis in IL-23 induced psoriasis model[98] indicate IMQ-induced Balb/c mice psoriasis model as a suitable platform to evaluate anti-psoriatic efficacy.

The mice in groups 1 and 2 were treated topically with Vaseline (negative control) and IMQ (62.5 mg/day; positive control) on the shaved back for 5 days. Whereas the mice in groups 3 and 4 were treated with sprayable NA3 loaded polymeric scaffold (equivalent to 800 μM NA3) and sprayable blank nanorod loaded polymeric scaffold (equivalent to 800 μM NA3), respectively post 8 h daily treatment with IMQ (62.5 mg/day) until 6 days (Fig. 6a and Supplementary Table 2). The mice were observed daily for indication of psoriatic scaling. It was observed that the psoriatic scaling on the mice back skin reduced in the order of IMQ treated (positive control) > blank nanorods scaffold > NA3 nanorods scaffold > Vaseline treated (negative control) (Supplementary Fig. 4a). The mice in each group were evaluated for erythema, scaling, and thickness using psoriatic area and severity index (PASI) scoring (Supplementary Table 3). It was observed that the cumulative PASI score of the mice in group 2 increased to 10.25 ± 1.25 on day 5. The cumulative score on day 5 was 0, 1.33 ± 0.577, and 0.66 ± 0.577 for mice in the negative control, Blank nanorod scaffold, and NA3 nanorod scaffold treated groups, respectively (Fig. 6b). No significant difference was observed in the body weight of the animals (Fig. 6c). The results corroborated previous findings that depicted species and strain-specific effects of IMQ-induced psoriasis on body weight[99]. The back thickness of mice treated with a blank nanorod-loaded polymeric scaffold decreased gradually compared with the NA3 nanorod-loaded polymeric scaffold, indicating higher efficacy of the NA3 nanorod-loaded polymeric scaffold (Fig. 6d). Prolonged inflammation causes an increase in the size and weight of the spleen. Interestingly, the spleen weight of the mice, when normalized against body weight in the NA3 nanorods polymeric scaffold and blank nanorods scaffold treated group, was significantly less ($p < 0.05$) compared with positive control (Fig. 6e). On day 6, the animals were euthanized, and the change in RNA expression levels relative to β-actin of NLRP3, AIM2, IL-1β, Caspase-1, and Gasdermin-D were evaluated from the back skin to elucidate the effect of NA3 nanorod/blank nanorod polymeric scaffold on NLRP3 and AIM2 inflammasomes. The results of qPCR corroborated with the in-vitro efficacy studies. Both NA3 nanorods polymeric scaffold and blank nanorods polymeric scaffold reduced the levels of caspase-1 and NLRP3 inflammasome, resulting in decreased IL-1β cytokine and gasdermin-D release compared with the positive control (Fig. 6f). The reduced inflammatory cytokine also reduced the T-cell recruiting CXCL2 chemokine levels. Although the nanorods were internalized using CD14 receptor, IMQ is endocytosed through TLR7 and TLR8 which enhances the Th17 cell recruitment and increased IL-17A cytokine[100]. The TLR 7 and 8 are also increased in presence of single stranded viral RNA and small synthetic compounds[101]. Therefore, we further studied the effect the blank nanorods/NA3 loaded nanorods scaffold on the TLR7 and TLR8. The upregulation of TLR7 was alleviated by 1.4-and 4.3-fold in blank nanorods polymeric scaffold and NA3 nanorods polymeric scaffold treated group, respectively compared with IMQ treated group (Fig. 6f). Additionally, the NA3 nanorods scaffold could alleviate the TLR8 by 1.8-fold compared with IMQ treated group (Fig. 6f). The enhanced efficacy of NA3 nanorods polymeric scaffold compared with blank nanorods polymeric scaffold was because of NA3 on AIM2 inflammasome and active caspase-1 where the blank nanorods lacked efficacy compared with positive control (Fig. 6f). Therefore, the RNA expression levels of AIM2 ($p < 0.01$), IL-1β ($p < 0.0001$), Caspase-1 ($p < 0.001$), CXCL2 ($p < 0.0001$), Gasdermin-D ($p < 0.001$), and TLR 7 and 8 ($p < 0.0001$) were significantly reduced in NA3 nanorods polymeric scaffold compared with blank nanorod polymeric scaffold treated mice skin. Moreover, IL-17A plays a central role in psoriatic inflammation, keratinocyte proliferation, hyperplasia, and microabscess formation providing a positive feedback loop in exacerbating immune response[102–104]. The Th17 cells in the psoriatic skin secrete IL-17A which attracts other inflammatory cells including the T-cells, natural killer cells, neutrophils, and mast cells[103]. Therefore, we analyzed the effect of NA3 nanorods on IL-17A where we observed IL-17A protein expression from the mice back skin treated with blank nanorods and NA3 nanorods was significantly reduced ($p < 0.05$) compared with IMQ treated mice back skin (positive control) when analyzed by western blot (Fig. 6g). Therefore, we hypothesize that targeting NLRP3 inflammasomes in macrophages (innate immune cells) serves as negative feedback loop to the Th17 cells reducing the TLR7, TLR8, and IL-17A levels. As expected, localized delivery led to no significant difference in the inflammasome activity systemically when confirmed with IL-1β levels in plasma samples (Supplementary Fig. 4b).

Psoriasis is a dermatological disorder involving epidermal hyperplasia and erythema[105]. The commencement of psoriasis includes edema in blood vessels and infiltration of neutrophils and lymphocytes[4]. Furthermore, it leads to parakeratosis due to incomplete maturation of keratinocyte retention of nuclei and release of extracellular lipids responsible for adhesion. Therefore, the stratum corneum becomes flaky. It involves the thickening of the epidermis, leading to acanthosis called Rete ridges. The severe form leads to hypogranulosis and migration of neutrophils in the intracorneal region into the stratum corneum called 'Munro abscess' and similar accumulation in the epidermis called 'pustule of Kogoj'[106,107]. The positive control (IMQ treated) mice depicted the characteristic features of psoriatic skin as per the H&E transverse section (Fig. 7a). On the contrary, faded rete ridges, inflammatory infiltration, and capillary inflammation were evident in blank nanorod-loaded polymeric scaffold-treated mice. The epidermal thickness and appearance were similar to negative control in NA3 nanorod-loaded polymeric scaffold-treated mice except for the presence of few inflammatory infiltrates (Fig. 7a).

The mitotic cell cycle phase is higher in psoriatic skin[108]. The Ki-67 are nuclear proteins that are increased in rapidly proliferating cells[109]. The immunohistochemical analysis of the 3,3′-Diaminobenzidine (DAB) antigen Keil 67 (Ki67) stained samples corroborated with the histopathological analysis. The DAB integrated density of IHC images was 1.8-folds higher in blank nanorods polymeric scaffold treated mice compared with NA3 nanorods polymeric scaffold. Therefore, the IHC analysis further uncovered the synergistic efficacy of NA3, nanorods, and mucin embedded in the polymeric scaffold (Fig. 7a, b). The H&E images and anti-CD31 DAB stained back skin transverse sections were analyzed microscopically to confirm the vascular hyperproliferation (Fig. 7a, c) and the extent of

https://doi.org/10.1038/s41467-024-53396-x

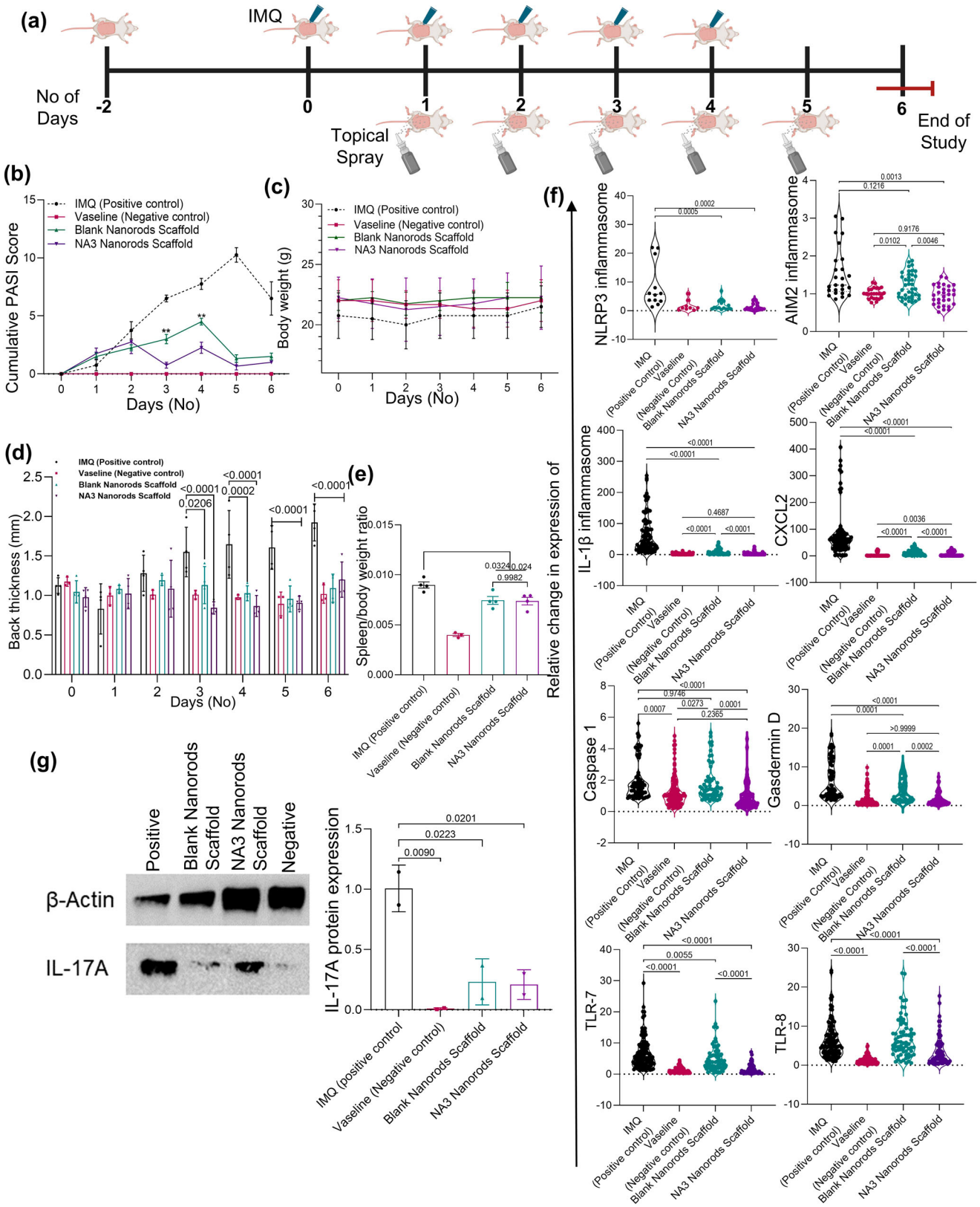


inflammatory cell infiltration (Fig. 7d and Supplementary Fig. 4f). It was observed that the inflammatory cell infiltrates were 2.1-fold and 4.1-fold lower in blank nanorods polymeric scaffold and NA3 nanorods polymeric scaffold treated mice, respectively when compared with the mice treated with IMQ (Fig. 7d). Moreover, the mean grey value of DAB stained anti-CD31 antibody was reduced by 1.6-folds in NA3 nanorods polymeric scaffold treated mice compared with IMQ treated mice (Fig. 7c). To conclude, despite the reduction in the NLRP3 inflammasome, the blank nanorod-loaded polymeric scaffold delayed the reduction in keratinocyte proliferation compared with the NA3 nanorod-loaded polymeric scaffold.

Existing anti-psoriatic therapy majorly consists of vitamin D3, retinoids, corticosteroids, calcineurin inhibitors, biologics, and phototherapy. Systemic, oral, and phototherapy are indicated for patients

**Fig. 6 | In-vivo evaluation in Imiquimod (IMQ) induced Psoriasis Balb/C mice model. a** Study paradigm schematic representation. Created in BioRender. Kulkarni, A. (2023) BioRender.com/h57d051. **b** Cumulative daily PASI score of back scaling, erythema, and thickness (Data represented as mean ± SEM, $n = 4$ for all other groups and 3 for negative control and analyzed by ANOVA and Tukey's multiple comparisons between NA3 nanorods and blank nanorods scaffold with ** indicates $p = 0.0075$). **c** Daily body weight measurement of IMQ-induced psoriasis mice in each group (Data represented as mean ± SD, $n = 4$ for all other groups and 3 for negative control). **d**, **e** Back thickness and spleen to body weight ratio of IMQ-induced mice from each group (Each data represented as mean ± SD; $n = 4$ for all other groups and 3 for negative control group; data analyzed by two-way ANOVA and Tukey's multiple comparisons). **f** RNA expression of different cellular components involved in NLRP3 and AIM-2 inflammasome activation extracted from the back skin of Balb/c mice in each group. (Each data represented for $n = 4$ for all other groups and 3 for negative control with 3 technical replicate per animal, data analyzed by Brown Forsythe and Welche one-way ANOVA Test). **g** Western blot analysis of IL-17A expressed in the mice back skin from each group (Each data represented as mean ± SD; $n = 4$, samples of 2 animals/sample were pooled and two different samples were run for western blot analysis, data analyzed by one-way ANOVA and Tukey's multiple comparison test). The uncropped gels are available in the supplementary and source data file.

eliciting failure to first-line topical therapy, and in case of moderate-to-severe psoriasis with a PASI area of >10%[110]. Phototherapy involves frequent physician visits decreasing patient compliance. Moreover, it could increase the risk of patient skin cancer and sensitivity to UV light. An increased susceptibility to secondary infections was observed due to systemic immunosuppression[111,112]. This leaves the topical localized anti-psoriatic therapy as a suitable treatment approach.

The topical therapy has been majorly explored to inhibit proliferation in T-cells and keratinocytes. The potent or super-potent corticosteroids that inhibit cell proliferation were considered suitable due to their efficacy[113]. However, corticosteroids increased the risk of adverse events including atrophy, striae, telangactiaceas, purpura, iatrogenic cushing syndrome, corticosteroid-related adison crises, growth retardation, mineralocorticoid effect[114,115], psoriatic relapse, and corticosteroid withdrawal symptoms[116] decreasing quality of life in psoriasis patients. Therefore, steroid-sparing agents were highly recommended and promoted for anti-psoriatic effects even if they would elicit delayed but consistent effects[113]. Other topical treatment regimens include vitamin D3 derivatives and retinoids targeting keratinocyte differentiation and proliferation[13,117]. Only, 14–50% clinical efficacy was obtained with vitamin D3 derivative or tazarotene (retinoid) monotherapy[113] due to their limitations including pH and UV-light sensitivity (Vitamin D3)[113], and erythema, pruritis, and burning associated with tazoretene[13]. Another approach includes T-cell targeted topical therapy including Calcineurin inhibitors. Various antibodies were developed with advances in the immunopathology of psoriasis. For instance, bimekizumab (IL-17A and IL-17F blocker) elicited clinical efficacy in 91% of psoriatic patients[118]. The development of antibodies against various receptors and cytokines would lead to an increased cost and unavoidable systemic immunomodulation. Given the drawbacks of existing therapies, there was an urgent need for a safe, efficacious, and cost-effective anti-psoriatic treatment. The majority of the existing drugs fail to target the inflammatory macrophages within psoriatic skin. The NA3 nanorod polymeric scaffolds decreased the IL-1β levels released by macrophages in psoriatic skin which would prevent further activation of Th17 keratinocyte proliferation[81,119]. Current work was directed toward the development of unique macrophage-targeted anti-psoriatic therapy which may elicit delayed yet consistent response. To avoid the repeatability as per the 3 R principle, considering the adverse effects of existing therapies, and the novelty of the developed NA3 nanorods polymeric scaffold, the blank nanorods polymeric scaffold and NA3 nanorods polymeric scaffold were compared with IMQ treated mice (positive control) to evaluate their ability to improve psoriasis in mice without causing systemic effects.

To conclude, the non-spherical LNPs were successfully developed, varying the molar ratio of PD and DSPE-PEG 2000 (carboxylic acid) from 2:1 to 10:1 by self-assembled thin-film hydration method. The morphology and stability of the nano-spheres/ellipses/rods were confirmed by transmission electron microscopy (TEM) and dynamic light scattering, respectively. The pathogen-like non-spherical trojan horse LNPs were internalized by macropinocytosis and clathrin-mediated endocytosis. The nanorods were internalized using CD14 while, the nanoellipses were internalized through TLR-4 receptors, respectively. The trojan-horse nanorods attenuated the NLRP3 inflammasomes due to the incorporation of PD. Moreover, it reduced ASC speck, lysosomal rupture, restrained calcium influx, and mitochondrial ROS formation. Developing a sprayable polymeric scaffold for delivering NA3-loaded nanorods elicited ease of administration, a simple manufacturing process, and synergistic inhibition of NLRP3 and AIM2 inflammasomes formation along with caspase-1 inhibition. The enhanced efficacy of the NA3 nanorod polymeric scaffold could be attributed to the combination effect of nanorods, NA3, and mucin. The evaluation of sprayable NA3-loaded nanorods in IMQ-induced psoriasis mice model depicted reduced psoriasis as confirmed by qPCR and immunohistopathology. Moreover, the reduced proliferation marker (Ki-67), vascularization, and inflammatory infiltrates confirmed the prodigious anti-psoriatic treatment potential of sprayable NA3-loaded nanorods polymeric scaffold. To conclude, non-spherical trojan horse nanorods incorporated within a sprayable polymeric scaffold were a novel platform delivery system with anti-inflammatory and anti-psoriatic properties. The sprayable NA3 nanorods-loaded polymeric scaffold paved the way for efficacious and localized delivery against psoriasis, eliminating drawbacks with existing therapies, including systemic immunosuppression and poor skin penetration. This approach could potentially revolutionize psoriasis therapy, eliciting benefits including ease of administration, tolerability, and scale-up. The novel prospects of the platform technology could be well explored for other inflammatory dermatological disorders with potential clinical translation.

## Methods

### Synthesis and characterization of nano-spheres/ellipses/rods

The self-assembled nano-spheres/ellipses/rods were obtained by thin film hydration coupled with ultrasonication with some modifications[55]. Briefly, pyridoxine-3,4-dipalmitate (PD) and DSPE-PEG(2000)carboxylic acid (DSPE-PEG 2000) were dissolved in dichloromethane and mixed in a round-bottomed flask at 2:1, 5:1, and 10:1 molar ratios for making nano-spheres, ellipses, and rods, respectively. The dichloromethane was evaporated at 90 °C under a vacuum on a Buchi® R-100 rotary flask evaporator to obtain a dried thin film. The dried film containing 2 mM PD was rehydrated using Milli-Q water at 90 °C. The rehydrated film was sonicated for 10 s at 40% amplitude using the FischerScientific probe sonicator (Model CL-18) and stirred at room temperature to obtain Nano-spheres/ellipses/rods.

DiD (0.067 mol% of total lipid concentration) dissolved in dichloromethane was added to PD and DSPE-PEG 2000 to prepare DiD-loaded Nano-spheres/ellipse/rods as per the aforementioned procedure.

### Particle size, PDI, and ζ-potential measurement

The Nano-spheres/ellipses/rods were diluted 100-folds using Milli-Q and the particle size and PDI were measured using a disposable sizing cuvette using a 637 nm laser at 173° backscattering angle on the Malvern Zetasizer ZSP (Malvern Instruments Ltd., UK) at 25 °C.

https://doi.org/10.1038/s41467-024-53396-x

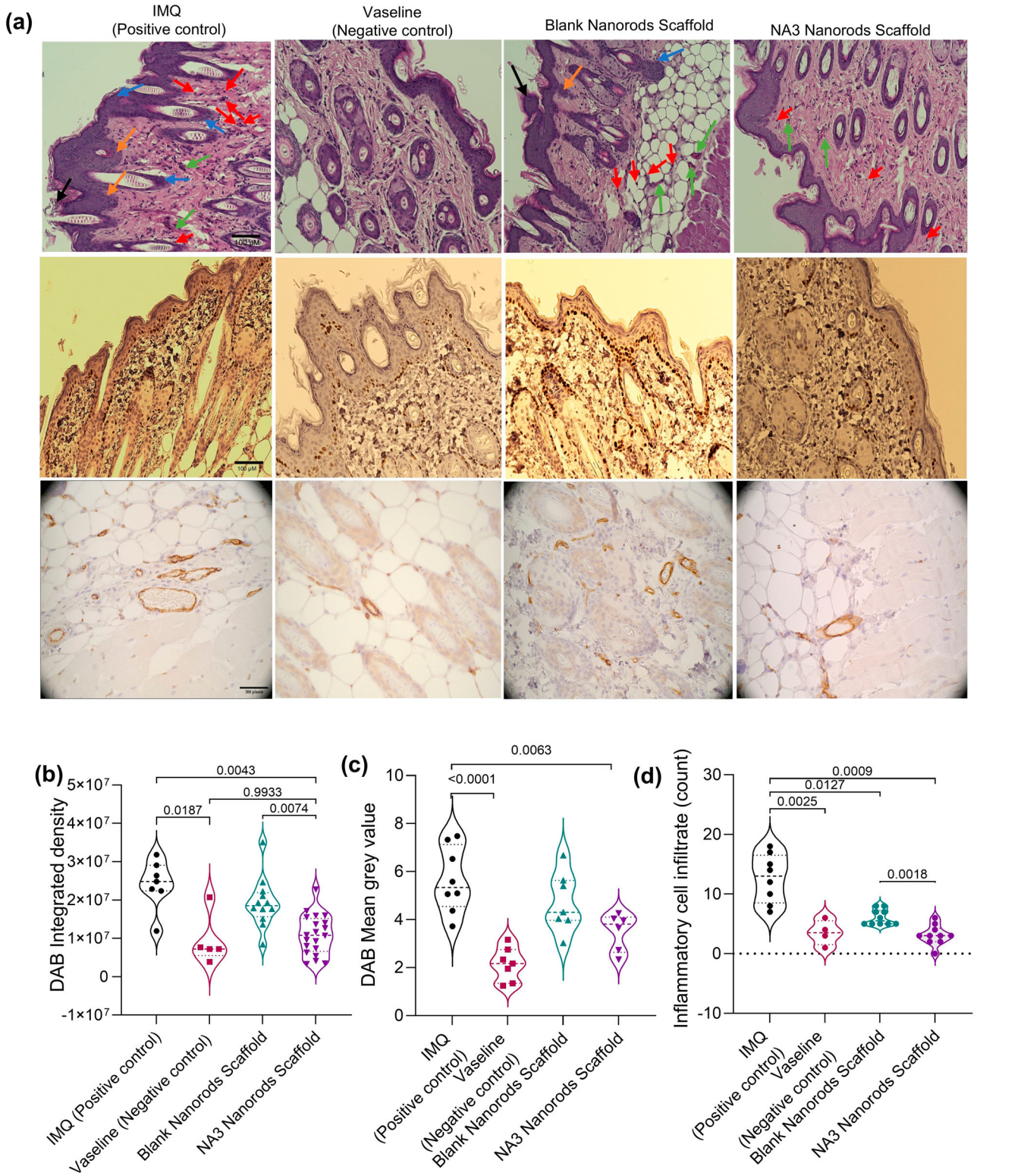


**Fig. 7 | Microscopic evaluation of in-vivo skin samples from Imiquimod (IMQ) induced Psoriasis Balb/C mice model. a** Light microscopic images of H&E, Ki67 (DAB), and CD31 antibody (DAB) stained preserved back skin transverse sections from euthanized mice on day 6 (Images represent Munro microabscess (black arrow), hyperplasia/hypogranulosis (blue arrow), Capillary proliferation (green arrow), Rete Ridges (orange arrow), Inflammatory infiltration (red arrow)). The H&E and DAB Ki 67 were analzyed at 20X (Scale bar: 100 μm) and the represented DAB CD31 were observed at 40X (scale bar: 300 pixels). **b** The integrated density of Ki67 DAB stain indicating cell proliferation measured from IHC sections imaged at 20X ($n = 4$ for all the groups and 3 for negative control group with 2 technical replicate for positive and negative control group and 3 technical replicates for blank and NA3 nanorods scaffold; data represented as mean ± SD; and analyzed by ordinary one-way ANOVA). **c** Mean grey value of CD31 marker indicating vascular hyperproliferation measured for IHC microscopic images at 20X and 40X (Data represented as mean ± S.D; $n = 4$ with 2 technical replicate per sample and analyzed by ordinary one-way ANOVA Tukey's multiple comparison) (**d**) The inflammatory cell infiltrate count indicating cell proliferation for H&E images at 40X ($n = 4$ with 2 technical replicate) (Data represented as mean ± SD; and analyzed by Brown Forsythe Welche Dunnet's T3 multiple comparison).

The ζ-potential of Nano-spheres/ellipses/rods was measured using disposable folded capillary cells (DST1070) on the Malvern Zetasizer ZSP (Malvern Instruments Ltd., UK) at 25 °C.

### Stability studies of nano-spheres/ellipse/rods

The prepared Nano-spheres/ellipses/rods were stored at 4 °C for 7 days. The stability of the nanoparticles was determined by measuring particle size, PDI, and zeta potential as mentioned above.

### Transmission electron microscopy

All spreads are done on freshly prepared carbon-stabilized Formvar support films on 200 mesh copper grids. The Nano-spheres, ellipses, and rods were absorbed into a carbon-coated Formvar support film for 30 s. Excess liquid was removed with filter paper and the sample was immediately negatively stained by running 6 drops of 1% uranyl acetate over the grid to contrast the spread samples. The excess stain was removed, and the sample was air-dried in a controlled humidity chamber (60% humidity). The samples were then examined using a ThermoFisher/FEI Tecnai 12 G2 transmission electron microscope and images were recorded using a Gatan Rio9, CMOS CCD camera system.

### Cell culture studies

iBMDMs with self-expressing ASC-CFP were thawed, diluted with DMEM cell culture media supplemented with 10% FBS and 1% Penicillin streptomycin (complete DMEM), and centrifuged using Thermo-Scientific centrifuge (Legend X1R, Waltham, USA) (355 g, 4 °C) for 5 min to obtain iBMDM pellet. The supernatant was discarded and the iBMDMs were split at a 1:6 ratio and cultured in a T25 flask by resuspending in complete DMEM in a $CO_2$ incubator (37 °C, 5% $CO_2$). The confluent iBMDMs were then passaged in a T-75 flask to obtain a cell count of 20 million cells/mL.

### Cytotoxicity studies by MTT assay

The cytotoxicity of the Nano-spheres/ellipses/rods was confirmed by MTT assay[120,121]. Briefly, iBMDMs (160,000 cells/well) were seeded in a 96-well plate overnight in a $CO_2$ incubator (37 °C, 5% $CO_2$). The Nano-spheres, ellipses, and rods were diluted with complete DMEM to yield 500 μM and 1000 μM total lipid concentration. The cells were treated with 100 μL Nano-spheres, ellipses, and rods (500 μM and 1000 μM), respectively for 24 h in an incubator (37 °C, 5% $CO_2$). The supernatant was then removed and the cells were incubated with 100 μL MTT reagent (500 μg/mL in PBS) for 4 h in a $CO_2$ incubator. The MTT reagent was removed and the formazan crystals were dissolved in 100 μL of cell culture grade DMSO for 1 h at room temperature. The absorbance was measured using Synergy HI BioTek microplate reader (Vermont, USA) at 570 nm to obtain the % cell viability using Eq. (1)

$$\%\,cell\ viability = \frac{Absorbance\ of\ cells\ treated\ with\ nanoparticles - Absorbance\ of\ blank}{Absorbance\ of\ untreated\ cell - Absorbance\ of\ blank} \times 100 \quad (1)$$

### Cellular uptake and internalization pathway by flow cytometry

The iBMDMs were counted using Trypan blue to obtain one million cells per well in a 12-well plate. The cells were pelleted by centrifugation and stained using 2 μM CSFE in 1X PBS for 20 min at 37 °C. Thereafter, the cells were separated by centrifugation and resuspended in complete DMEM. The CSFE-stained iBMDMs were seeded at $1 \times 10^6$ cells/ well in a 12-well plate overnight. The cells were treated with EIPA (100 μM), CPM (10 μg/mL), Dynasore (50 μg/mL), Cytochalasin D (2.5 μg/mL), and Nocodazole (5 μM) except in the control groups for 1 h. The supernatant was removed and the cells were washed with 1X PBS. Thereafter, DiD-loaded nano-spheres, ellipse, and rods, respectively (200 μM total lipid concentration) were added to the iBMDMs for 2 h. The supernatant was removed and the cells were washed with 1X PBS. The cells were then scraped, and centrifuged using ThermoScientific Legend Micro21R centrifuge (355 g, 4 °C, 5 min), and pellets were resuspended in 100 μL FACS staining buffer. The cellular uptake was quantified using an ACEA novocyte flow cytometer. The double-positive cells were gated using Novoexpress 1.2.5 software and the fluorescent intensity of APC in the double-positive quadrant was plotted in GraphPad Prism (version 9.3.1).

### Cellular internalization by CD14 and TLR-4 determined by flow cytometry

The iBMDMs were seeded in 12 well plate ($1 \times 10^6$ cells/well). The cells in each well were treated with FITC anti-CD14 antibody (Biolegend, Cat no.: 123307, clone name: Sa14-2, lot no.: B410733; dilution: 1:100) for 30 min to block the CD14 receptors while, the cells without treatment of FITC anti-CD14 antibody (1:100 dilution) served as control. The cells were washed and then treated with DiD loaded nano-spheres/ellipses/rods (200 μM total lipid concentration) for 4 h. A group of cells without treatment of lipid nanoparticles but stained for anti-CD14 antibody served as control. The supernatant was removed and the cells were washed with 1X PBS. The cells were then scraped, and centrifuged using ThermoScientific Legend Micro21R centrifuge (355 *g*, 4 °C, 5 min), and pellets were resuspended in 100 μL FACS staining buffer. The gating was done using Novoexpress 1.2.5 software and the fluorescent intensity of APC-positive cells was plotted in GraphPad Prism (version 9.3.1).

The involvement of TLR-4 in the internalization of Trojan-horse LNP and the iBMDMs were treated with 1000 μM of nano-spheres/ellipses/rods respectively. Thereafter, the supernatant was removed and the cells were scraped and separated by centrifugation (355 g, 5 min). The RNA was extracted using Trizol reagent based on the manufacturer's protocol and the purity was assessed using Nanodrop. The total TLR-4 RNA was reverse transcribed using the high-capacity cDNA reverse transcriptase kit according to the manufacturer's protocol. The qPCR was performed using Taqman Fast Advanced MasterMix and Taqman gene expression assay as per manufacturer protocol. The gene expression was normalized by β-actin mRNA.

### IL-1β levels by ELISA

iBMDMs ($1.6 \times 10^5$ cells/ well) were seeded in a 96-well plate overnight. The cells were treated with 100 μL nano-spheres, ellipses, and rods, respectively (500 μM and 1000 μM total lipid concentration) for 24 h. Thereafter, the supernatant was removed and the cells were primed with 200 μL lipopolysaccharide (100 ng/mL) for 4 h. Later, the supernatant was removed and the cells were treated with 100 μL Nigericin (10 μM) for 2 h. The supernatant was removed and added to the 96-well plate which was previously coated with capture antibody and blocked with ELISA spot buffer. The IL-1$\beta$ released by individual groups was determined by performing the ELISA as per the Invitrogen Corporation manufacturer's instruction.

### ASC speck and lysosomal rupture by confocal fluorescent microscopy

iBMDMs expressing CFP-ASC were seeded in an 8-well chamber slide ($0.8 \times 10^6$ cells/well) overnight. For ASC speck determination, the cells were treated with 100 μL of nano-spheres, ellipses, and rods for 12 h. Thereafter, the cells were washed with 1X PBS and treated with 200 μL/well LPS followed by 100 μL/well Nigericin (10 μM) for 4 h and 1 h, respectively. The cells were incubated at 37 °C for 15 min with complete DMEM media containing NucBlue (2 drops/ mL) and Propidium Iodide (2 μg/mL) and imaged at 20X magnification using CREST v2 TIRF Spinning Disc Confocal Microscope. The data were quantified using Nikon NIS element AR software.

For the lysosomal rupture assay, the cells were treated with 200 μM DiD-loaded nano-spheres, ellipse, and rods for 2 h before

200 μL LPS (100 ng/mL) and 10 μM Nigericin treatment for 4 h and 1 h, respectively. Thereafter, the cells were treated with NucBlue (2 drops per mL) and LysoTracker Red DND-99 (0.1 μM) at 37 °C for 30 min. Later, the cells were washed and treated with media containing NucBlue for imaging and quantification.

### Calcium influx and mitochondrial ROS levels by flow cytometry

The iBMDMs ($1 \times 10^6$ cells/well) were seeded in a 12-well plate overnight. The cells were treated with 1 mM of nano-spheres, ellipses, and rods for 4 h. Thereafter, the cells were washed with 1X PBS and treated stained with Fluo-4 AM or MitoSox Red in complete CPBS (with Calcium chloride and Magnesium chloride) and HBSS, respectively for 20 min at 37 °C for 30 min. Later the cells were washed and scraped in 1X PBS/HBSS. The cells were separated by centrifugation, resuspended in 100 μL FACS buffer and processed by ACEA novocyte flow cytometer. The FITC and PE-positive cells were quantified to determine the calcium influx and mitochondrial ROS production, respectively. The FITC or PE fluorescent intensity was plotted in GraphPad Prism (version 10).

### Synthesis of NA3 nanorods and NA3 nanorods polymeric scaffold

NA3, PD, and DSPE-PEG 2000 COOH in the molar ratio of 20:10:1 were dissolved in DCM (1 mL). The DCM solution was added to a round bottom flask (RBF) to form a thin film on the rotary flask evaporator (90 °C, 10 min). The thin film was rehydrated using Milli-Q (1 mL, 90 °C). The rehydrated solution was subjected to bath sonication (7 s, 60 °C) and probe sonication (7 s, 90 °C, 40% amplitude, 7 s on and off cycle). The formulation was kept under stirring until it reached room temperature. The free NA3 was separated by centrifugation (14,084 *g* for 5 min) and the NA3-loaded nanorod in the supernatant was collected and analyzed by RP-HPLC to analyze % drug loading and % entrapment efficiency.

The NA3 nanorods polymeric scaffold was synthesized using Poloxamer 407 (10% w/v) and mucin (2.5 mg/mL) which were added to NA3 nanorods (1 mL) and stirred to obtain a clear solution. Only Poloxamer 407 (10% w/v) was added to blank nanorods to obtain blank nanorods polymeric scaffold. The scaffold was further analyzed to obtain the NA3 content using the RP-HPLC method.

### Characterization of NA3/Blank nanorods loaded polymeric scaffold

The NA3/blank nanorods and their polymeric scaffold were diluted 100-folds using Milli-Q and the particle size and PDI were measured using a disposable sizing cuvette using a 637 nm laser at 173° backscattering angle on the Malvern Zetasizer ZSP (Malvern Instruments Ltd., UK) at 25 °C. The ζ-potential of the NA3/blank nanorods and their polymeric scaffold was measured using disposable folded capillary cells (DST1070) on the Malvern Zetasizer ZSP (Malvern Instruments Ltd., UK) at 25 °C. The Blank/NA3 nanorods and their polymeric scaffold were stored at 4 °C for 7 days. The stability of the nanoparticles was determined by measuring particle size, PDI, and zeta potential as mentioned above.

The NA3 % entrapment efficiency, % drug loading in nanorods, and the NA3 content in NA3 nanorod polymeric scaffold was analyzed by RP-HPLC method. The stationary phase consisted of a sunfire C18 column (4.6 × 150 mm) and the mobile phase consisted of 0.1% TFA in acetonitrile and Milli-Q (A&B). The RP-HPLC method involved gradient elution with %A and %B of 5% and 95% at the initial time point. The gradient was switched to 95:5(%A:%B) in 1 min and continued until 7 min, The gradient was reversed to 5:95 (%A:%B) from 7–12 min. The mobile phase was pumped at a 1 ml/min flow rate using a quaternary gradient pump in the Waters® HPLC system with the manual injector.

### In vitro characterization of NA3/blank nanorods and NA3/blank nanorods loaded polymeric scaffold

iBMDMs ($1.6 \times 10^5$ cells/ well) were seeded in a 96-well plate overnight. The cells were treated with 100 μL NA3 nanorods/blank nanorods, free NA3, NA3/blank nanorods loaded polymeric scaffold (equivalent to 200 μM, 100 μM, 50 μM NA3) for 24 h. Thereafter, the supernatant was removed and the cells were primed with 200 μL lipopolysaccharide (100 ng/mL) for 4 h. Later, the supernatant was removed and the cells were treated with 100 μL Nigericin (10 μM) and/or 100 μL Nigericin (10 μM) and Poly (dA:dT) (2.5 μg/mL) for 2 h. The supernatant was removed and added to the 96-well plate which was previously coated with capture antibody and blocked with ELISA spot buffer. The IL-1$\beta$ released by individual groups was determined by performing the ELISA as per the Invitrogen Corporation manufacturer's instruction.

iBMDMs expressing CFP-ASC were seeded in an 8-well chamber slide ($0.8*10^6$ cells/well) overnight. For ASC speck determination, the cells were treated with 100 μL of NA3 nanorods/blank nanorods, free NA3, and NA3/blank nanorods loaded polymeric scaffold (equivalent to 200 μM NA3) for 12 h. Thereafter, the cells were washed with 1X PBS and treated with 200 μL/well LPS followed by 100 μL/well Nigericin (10 μM) for 4 h and 1 h, respectively. The cells were incubated at 37 °C for 15 min with complete DMEM media containing NucBlue (2 drops/ mL) and Propidium Iodide (2 μg/mL) and imaged at 20X magnification using CREST v2 TIRF Spinning Disc Confocal Microscope. The data were quantified using Nikon NIS element AR software.

### In-vitro drug release studies

NA3 nanorods loaded polymeric scaffold were suspended in Milli-Q or iBMDM cell lysate (pH 5-6) and filled in a dialysis bag (1000 Da molecular weight cut off). The dialysis bags were suspended in PBS (pH 7.4;10 mL) and kept under stirring (350 rpm, 37 °C) to mimic sink condition. An aliquot (0.5 mL) was withdrawn at pre-determined time points and replenished with equivalent fresh PBS. The cumulative drug release was analyzed by the RP-HPLC method.

### Western blot analysis

iBMDMs ($3.2 \times 10^6$ cells) were seeded in petri-plate (60 mm diameter). The cells were treated with NA3 nanorods loaded polymeric scaffold (equivalent to 200 μM NA3; 2 mL) and blank nanorods polymeric scaffold (equivalent to NA3 nanorods; 2 mL) for 24 h. The supernatant was removed and the cells were treated with LPS (100 ng/mL; 2 mL) for 4 h followed by Nigericin (10 μM, 2 mL) for 1 h. The supernatant was removed and cells were washed with 2 mL 1X PBS and lysed using 1X HALT protease and phosphatase inhibitor in RIPA lysis buffer. Samples were kept on ice and vortexed every 5 min for 30 min. Samples were then sonicated in a water bath for 10 s for 90 s and centrifuged at 14,084 *g* for 15 min. The supernatant was removed and put into a new tube to be frozen at −80 °C. For western blot analysis of animal samples, tissues were homogenized in 2 mL 1X HALT protease and phosphatase inhibitor in RIPA lysis buffer. After homogenization samples were prepared as previously described for in vitro samples.

The protein content in each group was determined by BCA assay and samples containing equal amounts of protein lysates were electrophoresed on a 10% polyacrylamide gel. The gel was transferred onto the PVDF membrane followed by blocking for 2 h in TBST (5% skim milk). The membranes were incubated in 1% BSA in TBST with caspase-1 (1:1000 dilution) antibody (Rabit IgG by Cell signaling technology®, catalogue no.:24232S, clone no.:N/A, lot no.:4), β-actin (Source: Rabit IgG by Cell signaling technology®, Catalogue no.: 4970S, clone no.: N/A, lot no.: 19, Dilution: 1:1000) and IL-17A antibody (Rabit IgG by Cell signaling technology®, catalogue no.:13838S, clone no.: N/A, lot no.:4, Dilution: 1:1000) (for tissue samples) overnight at 4°C. The membranes

were then washed with TBST and incubated with horseradish peroxidase-conjugated secondary antibody (1:2000 dilution) (Source: Mouse IgG by Santa Cruz Animal Health, catalogue no.: 516102, Clone no.:N/A, lot no.: E2318) for 1 h at room temperature. Detection was done using Biorad Clarity ECL and the images were processed by Image J. The uncropped and unprocessed images of the blot are represented in Supplementary Fig. 6f.

### Rheological behavior of NA3 nanorods loaded polymeric scaffold by parallel plate rheology

The storage and loss moduli (G′ and G″ respectively) of poloxamer solutions and nanoparticle formulations were determined on a Netzsch Kinexus parallel plate rheometer and used to find the gel transition temperature. Measurements were run on a 20 mm flat plate with a 1 mm plate gap and a solvent trap to prevent water evaporation at elevated temperatures from affecting the data. A temperature table from 25 to 50 °C was constructed by running a frequency sweep from 0.1–10 Hz at 1% strain followed by an amplitude sweep from 0.1 to 10% strain at 1 Hz, incrementing the temperature by 1 °C after each pair of sweeps. The gel point was defined using the Winter-Chambon criterion, for which the gel point is defined as the point at which $tan\delta$ becomes frequency independent at small frequencies. Rheological experiments were analyzed using IRIS Rheo-Hub.

### In-vivo studies in Psoriatic Balb/c mice

Female Balb/c mice were housed at ambient temperature with 70% relative humidity in the institute animal house and provided with 12 h light and dark cycle. The Balb/c mice (total: 15; 4–6 weeks old) were divided into four groups ($n = 4$ each) and their back was shaved two days before the study. The differences in the sex was not considered in this study since the aim of the in-vivo study was to establish proof of concept of the developed sprayable polymeric scaffold loaded with NA3 nanorods. Moreover, the difference in the skin thickness would not be a major concern since we aim to develop a topical therapy devoid of systemic effect. The mice in group 1 were untreated (negative control, $n = 3$). Imiquimod topical cream (5% w/w; 62.5 mg per mouse) was applied on the back of every mouse in the rest of the groups for 5 consecutive days. Two groups were treated with blank nanorods (suspended in Poloxamer 407 (10% w/v) topical spray and NA3 loaded nanorods (suspended in Poloxamer 407 (10% w/v)) and mucin (2.5 mg/mL) topical spray), respectively for 5 days post Imiquimod treatment. The efficacy was evaluated using the psoriatic area and severity index scoring for 5 days. The body weight, back thickness, scaling, and erythema were evaluated every day for 6 days. The mice were sacrificed on day 6 and the skin was minced and analyzed for cellular inflammatory and proliferation markers including NLRP3, AIM2, IL-1β, CXCL2, Caspase-1, TLR7, TLR8, and Gasdermin-D. The remaining skin was processed for immunohistochemistry of Ki-67 proliferation marker, CD31 vascular proliferation marker as per manufacturers protocol, and hematoxylin and Eosin staining (H&E)[28]. The study protocol was approved by University of Massachusetts, Amherst IACUC committee (protocol no.: 4895).

### qPCR analysis of skin samples

**RNA extraction.** Skin tissue (50–100 mg) was minced and homogenized for 1 min in Trizol (1 mL), vortexed, and incubated at 37 °C for 20 min. Chloroform (200 μL) was added, vortexed, and sample was incubated at 37 °C for 2-3 min. All samples were centrifuged at 12,000 *g* for 15 min. The clear solution was separated and isopropanol (500 μL) was added as well as 0.5 μL RNA grade glycogen, vortex, and store at 4 °C for 10 min. The sample was centrifuged at 12,000 *g* for 10 min and pellet was collected. One mL ethanol (75% v/v) was added to each sample, vortexed, and centrifuged at 7500 g for 5 min, discarding the supernatant. Allow the Eppendorf to air dry for 5 to 10 min. Add 20 μL RNA-free water and place sample in 55–60 °C water bath for 10 to 15 min. RNA concentration and purity were measured using Nanodrop. Total RNA was reverse transcribed using the High-Capacity cDNA Reverse Transcriptase Kit (Applied Biosystems) according to the manufacturer's protocol[122].

**qPCR.** qPCR was performed with TaqMan Fast Advanced Master Mix and TaqMan Gene Expression Assay (FAM) following the manufacturer's protocols. Relative transcription was normalized for that of β-actin mRNA. Information about the qPCR primers is provided in Supplementary Supplementary Table 1.

### Histopathological evaluation of psoriatic skin specimens

The psoriatic skin sections were flash-frozen in OCT. Thin sections (5 μM) of the tissue were obtained and stained with hematoxylin-eosin stain, DAB Ki-67 antibody (Abcam ab16667, Dilution 1:100, AR: pH6 10 min, clone no.SP6, catalogue no. ab16667, lot no. GR3255131-11), and DAB CD31 antibody (Source: Abcam, dilution: 1:2000, clone no.: EPR17259, catalogue no: ab182981, lot no.: GR3341007-16). The stained sections were then mounted and imaged on a Keyence BZ-X810 light microscope. The images were analyzed by Image J.

### Statistical analysis

The in-vitro an in-vivo statistical analysis has been done using both technical and biological replicates. Specific statistical tests applied for the analysis are mentioned in the figure caption.

### Reporting summary

Further information on research design is available in the Nature Portfolio Reporting Summary linked to this article.

## Data availability

The authors declare that all data supporting the findings of this study are available within the paper and its Supplementary Information. The additional data as requested will be provided by the corresponding author. Source Data is available for Figs. 2(a, c–f), 3(c, f–i), 4(b–g), 5(a–i), 6(b–g), 7(b–d), and Supplementary Figs. 1(b, c), 4(c–e), 6(a–d) in associated source data file. Source data are provided with this paper.

## References

1. Armstrong, A. W. & Read, C. Pathophysiology, Clinical Presentation, and Treatment of Psoriasis: A Review. *JAMA - J. Am. Med. Assoc.* **323**, 1945–1960 (2020).
2. *Global Report on Psoriasis*; 2016.
3. Rendon, A. & Schäkel, K. Psoriasis Pathogenesis and Treatment. *Int. J. Mol. Sci.* **20**, 1–28 (2019).
4. Yamanaka, K., Yamamoto, O. & Honda, T. Pathophysiology of Psoriasis: A Review. *J. Dermatol.* **48**, 722–731 (2021).
5. Zhou, X., Chen, Y., Cui, L., Shi, Y., Guo, C. Advances in the Pathogenesis of Psoriasis: From Keratinocyte Perspective. *Cell Death Dis*. **13** https://doi.org/10.1038/s41419-022-04523-3 (2022).
6. Verma, D. et al. Enhanced Inflammasome Activity in Patients with Psoriasis Promotes Systemic Inflammation. *J. Invest. Dermatol.* **141**, 586–595.e5 (2021).
7. Ciążyńska, M. et al. The Role of NLRP1, NLRP3, and AIM2 Inflammasomes in Psoriasis: Review. *Int. J. Mol. Sci.* **22**, 1–11 (2021).
8. Wang, H. et al. Targeting NF-KB with a Natural Triterpenoid Alleviates Skin Inflammation in a Mouse Model of Psoriasis. *J. Immunol.* **183**, 4755–4763 (2009).
9. Nowowiejska, J. et al. Gasdermin D (GSDMD) Is Upregulated in Psoriatic Skin—A New Potential Link in the Pathogenesis of Psoriasis. *Int. J. Mol. Sci*. **24** https://doi.org/10.3390/ijms241713047 (2023).
10. Stanescu, A. M. A., Simionescu, A. A. & Diaconu, C. C. Oral Vitamin D Therapy in Patients with Psoriasis. *Nutrients* **13**, 1–12 (2021).

11. Sadeghinia, A. & Daneshpazhooh, M. Immunosuppressive Drugs for Patients with Psoriasis during the COVID-19 Pandemic Era. A Review. *Dermatol. Ther.* **34**, 1–9 (2021).
12. Jiang, Y., Chen, Y., Yu, Q. & Shi, Y. Biologic and Small-Molecule Therapies for Moderate-to-Severe Psoriasis: Focus on Psoriasis Comorbidities. *BioDrugs* **37**, 35–55 (2023).
13. Timis, T. L., Florian, I. A., Vesa, S. C., Mitrea, D. R., Orasan, R. I. *An Updated Guide in the Management of Psoriasis for Every Practitioner;* Vol. 75. https://doi.org/10.1111/ijcp.14290 (2021).
14. Szymański, Ł. et al. Retinoic Acid and Its Derivatives in Skin. *Cells* **9**, 1–14 (2020).
15. van de Kerkhof, P. C. M. & de Gruijl, F. R. Phototherapy in the Perspective of the Chronicity of Psoriasis. *J. Eur. Acad. Dermatol. Venereol.* **34**, 926–931 (2020).
16. Bos, J. D. & Spuls, P. I. Topical Treatments in Psoriasis: Today and Tomorrow. *Clin. Dermatol.* **26**, 432–437 (2008).
17. Vanaja, S. K., Rathinam, V. A. K. & Fitzgerald, K. A. Mechanisms of Inflammasome Activation: Recent Advances and Novel Insights. *Trends Cell Biol.* **25**, 308–315 (2015).
18. Nandi, D., Farid, N. S. S., Karuppiah, H. A. R. & Kulkarni, A. Imaging Approaches to Monitor Inflammasome Activation. *J. Mol. Biol.* **434**, 167251 (2022).
19. Tan, R. Zhi. et al. Macrophages Mediate Psoriasis via Mincle-Dependent Mechanism in Mice. *Cell Death Discov.* **9** https://doi.org/10.1038/s41420-023-01444-8 (2023).
20. He, X. et al. Prokineticin 2 Plays a Pivotal Role in Psoriasis. *EBioMedicine* **13**, 248–261 (2016).
21. Tu, Q. et al. Prokineticin 2 Promotes Macrophages-Mediated Antibacterial Host Defense against Bacterial Pneumonia. *Int. J. Infect. Dis.* **125**, 103–113 (2022).
22. Davies, L. C. et al. Distinct Bone Marrow-Derived and Tissue-Resident Macrophage Lineages Proliferate at Key Stages during Inflammation. *Nat. Commun.* **4** https://doi.org/10.1038/ncomms2877 (2013).
23. Yang, L. et al. Hsa_circ_0004287 Inhibits Macrophage-Mediated Inflammation in an N6-Methyladenosine–Dependent Manner in Atopic Dermatitis and Psoriasis. *J. Allergy Clin. Immunol.* **149**, 2021–2033 (2022).
24. Zahid, A., Li, B., Kombe, A. J. K., Jin, T. & Tao, J. Pharmacological Inhibitors of the Nlrp3 Inflammasome. *Front. Immunol.* **10**, 1–10 (2019).
25. Tuoda, M. A. T., Tu, M., Ana, A. T. A., Att, T., Hati, H. A. N. Lipid Nanoparticles Comprising Lipophilic Anti - Inflammatory Agents and Methods of Use Thereof. **1** (2017).
26. Dipika, N., Maharshi, D., James, F. I., Ankit, P., Ashish, K. Nanoparticle-Mediated Co-Delivery of Inflammasome Inhibitors Provide Protection against Sepsis. *Nanoscale*. https://doi.org/10.1039/D3NR05570A (2024).
27. Wang, L. et al. Hyaluronic Acid Nanoparticles as a Topical Agent for Treating Psoriasis. *ACS Nano* **16**, 20057–20074 (2022).
28. Tsuji, G. et al. Metformin Inhibits IL-1β Secretion via Impairment of NLRP3 Inflammasome in Keratinocytes: Implications for Preventing the Development of Psoriasis. *Cell Death Discov.* **6** https://doi.org/10.1038/s41420-020-0245-8 (2020).
29. Deng, G. et al. Inhibition of NLRP3 Inflammasome-Mediated Pyroptosis in Macrophage by Cycloastragenol Contributes to Amelioration of Imiquimod-Induced Psoriasis-like Skin Inflammation in Mice. *Int. Immunopharmacol.* **74**, 105682 (2019).
30. Chung, I. C. et al. EFLA 945 Restricts AIM2 Inflammasome Activation by Preventing DNA Entry for Psoriasis Treatment. *Cytokine* **127**, 154951 (2020).
31. Qiao, P. et al. Quinolinic Acid, a Tryptophan Metabolite of the Skin Microbiota, Negatively Regulates NLRP3 Inflammasome through AhR in Psoriasis. *J. Invest. Dermatol.* **142**, 2184–2193.e6 (2022).
32. Gaire, B. P. et al. Lysophosphatidic Acid Receptor 5 Contributes to Imiquimod-Induced Psoriasis-Like Lesions through NLRP3 Inflammasome Activation in Macrophages. *Cells* **9** https://doi.org/10.3390/cells9081753 (2020).
33. Zamansky, M., Yariv, D., Feinshtein, V., Ben-Shabat, S. & Sintov, A. C. Cannabidiol-Loaded Lipid-Stabilized Nanoparticles Alleviate Psoriasis Severity in Mice: A New Approach for Improved Topical Drug Delivery. *Molecules* **28**, 1–16 (2023).
34. Rahmanian-Devin, P. et al. Preparation and Characterization of Solid Lipid Nanoparticles Encapsulated Noscapine and Evaluation of Its Protective Effects against Imiquimod-Induced Psoriasis-like Skin Lesions. *Biomed. Pharmacother.* **168**, 115823 (2023).
35. Tenchov, R., Bird, R., Curtze, A. E. & Zhou, Q. Lipid Nanoparticles from Liposomes to MRNA Vaccine Delivery, a Landscape of Research Diversity and Advancement. *ACS Nano* **15**, 16982–17015 (2021).
36. Hou, X., Zaks, T., Langer, R. & Dong, Y. Lipid Nanoparticles for MRNA Delivery. *Nat. Rev. Mater.* **6**, 1078–1094 (2021).
37. Maharshi, D., James, F. I., Anujan, R. & Kulkarni, A. Protein Corona Formation on Lipid Nanoparticles Negatively Affects the NLRP3 Inflammasome Activation. *Bioconjug. Chem.* **34**, 1766–1779 (2023).
38. Forster, J., Nandi, D. & Kulkarni, A. MRNA-Carrying Lipid Nanoparticles That Induce Lysosomal Rupture Activate NLRP3 Inflammasome and Reduce MRNA Transfection Efficiency. *Biomater. Sci.* **10**, 5566–5582 (2022).
39. Li, T. et al. Lysine-Containing Cationic Liposomes Activate the NLRP3 Inflammasome: Effect of a Spacer between the Head Group and the Hydrophobic Moieties of the Lipids. *Nanomed. Nanotechnol., Biol. Med.* **14**, 279–288 (2018).
40. Lonez, C. et al. Cationic Lipid Nanocarriers Activate Toll-like Receptor 2 and NLRP3 Inflammasome Pathways. *Nanomed. Nanotechnol., Biol. Med.* **10**, 775–782 (2014).
41. Granot, Y. & Peer, D. Delivering the Right Message: Challenges and Opportunities in Lipid Nanoparticles-Mediated Modified MRNA Therapeutics—An Innate Immune System Standpoint. *Semin. Immunol.* **34**, 68–77 (2017).
42. Lee, Y., Jeong, M., Park, J., Jung, H. & Lee, H. Immunogenicity of Lipid Nanoparticles and Its Impact on the Efficacy of MRNA Vaccines and Therapeutics. *Exp. Mol. Med.* **55**, 2085–2096 (2023).
43. Zhu, X. et al. Loss of NLRP3 Reduces Oxidative Stress and Polarizes Intratumor Macrophages to Attenuate Immune Attack on Endometrial Cancer. *Front. Immunol.* **14**, 1–10 (2023).
44. Ni, D. et al. Biomimetically Engineered Demi-Bacteria Potentiate Vaccination against Cancer. *Adv. Sci.* **4**. https://doi.org/10.1002/advs.201700083 (2017).
45. Doshi, N. & Mitragotri, S. Macrophages Recognize Size and Shape of Their Targets. *PLoS One* **5**, 1–6 (2010).
46. Dhar, P. & McAuley, J. The Role of the Cell Surface Mucin MUC1 as a Barrier to Infection and Regulator of Inflammation. *Front. Cell. Infect. Microbiol.* **9**, 1–8 (2019).
47. Ciesielska, A., Matyjek, M. & Kwiatkowska, K. TLR4 and CD14 Trafficking and Its Influence on LPS-Induced pro-Inflammatory Signaling. *Cell. Mol. Life Sci.* **78**, 1233–1261 (2021).
48. Nejadmansouri, M., Eskandari, M. H., Yousefi, G. H., Riazi, M. & Hosseini, S. M. H. Promising Application of Probiotic Microorganisms as Pickering Emulsions Stabilizers. *Sci. Rep.* **13**, 1–18 (2023).
49. Tang, L. & Zhou, F. Inflammasomes in Common Immune-Related Skin Diseases. *Front. Immunol.* **11**, 1–15 (2020).
50. Zhang, P. et al. Vitamin B6 Prevents IL-1β Protein Production by Inhibiting NLRP3 Inflammasome Activation. *J. Biol. Chem.* **291**, 24517–24527 (2016).
51. Paolino, D. et al. Interaction between PEG Lipid and DSPE/DSPC Phospholipids: An Insight of PEGylation Degree and Kinetics of de-PEGylation. *Colloids Surf. B Biointerfaces* **155**, 266–275 (2017).

52. Higashi, K. et al. Composition-Dependent Structural Changes and Antitumor Activity of ASC-DP/DSPE-PEG Nanoparticles. *Eur. J. Pharm. Sci.* **99**, 24–31 (2017).
53. Kowalska, M., Broniatowski, M., Mach, M., Płachta, Ł. & Wydro, P. Effect of Lipopolymer (DSPE-PEG750) on Phospholipid Monolayers and Bilayers Differing in the Structure of the Polar Head Group. *J. Mol. Liq.* **344**, 117715 (2021).
54. Kowalska, M., Broniatowski, M., Mach, M., Płachta, Ł. & Wydro, P. The Effect of the Polyethylene Glycol Chain Length of a Lipopolymer (DSPE-PEGn) on the Properties of DPPC Monolayers and Bilayers. *J. Mol. Liq.* **335**, 116529 (2021).
55. Chen, Z. et al. Understanding the Rod-to-Tube Transformation of Self-Assembled Ascorbyl Dipalmitate Lipid Nanoparticles Stabilized with PEGylated Lipids. *Nanoscale* **15**, 2602–2613 (2022).
56. Chen, Z. et al. The Nanostructure of Rod-like Ascorbyl Dipalmitate Nanoparticles Stabilized by a Small Amount of DSPE-PEG. *Int. J. Pharm.* **602**, 120599 (2021).
57. Ferreira, S. A., Correia, A., Madureira, P., Vilanova, M. & Gama, F. M. Unraveling the Uptake Mechanisms of Mannan Nanogel in Bone-Marrow-Derived Macrophages. *Macromol. Biosci.* **12**, 1172–1180 (2012).
58. Vasudevan, S. O., Russo, A. J., Kumari, P., Vanaja, S. K. & Rathinam, V. A. A TLR4-Independent Critical Role for CD14 in Intracellular LPS Sensing. *Cell Rep.* **39**, 110755 (2022).
59. Zanoni, I., Tan, Y., Di Gioia, M., Springstead, J. R. & Kagan, J. C. By Capturing Inflammatory Lipids Released from Dying Cells, the Receptor CD14 Induces Inflammasome-Dependent Phagocyte Hyperactivation. *Immunity* **47**, 697–709.e3 (2017).
60. Madej, M. P., Töpfer, E., Boraschi, D. & Italiani, P. Different Regulation of Interleukin-1 Production and Activity in Monocytes and Macrophages: Innate Memory as an Endogenous Mechanism of IL-1 Inhibition. *Front. Pharmacol.* **8**, 1–12 (2017).
61. Nandi, D. et al. Core Hydrophobicity of Supramolecular Nanoparticles Induces NLRP3 Inflammasome Activation. *ACS Appl. Mater. Interfaces* **13**, 45300–45314 (2021).
62. Yang, Y., Wang, H., Kouadir, M., Song, H., Shi, F. Recent Advances in the Mechanisms of NLRP3 Inflammasome Activation and Its Inhibitors. *Cell Death Dis.* **10** https://doi.org/10.1038/s41419-019-1413-8 (2019).
63. Makvandi, P. et al. Non-Spherical Nanostructures in Nanomedicine: From Noble Metal Nanorods to Transition Metal Dichalcogenide Nanosheets. *Appl. Mater. Today* **24**, 101107 (2021).
64. Lin, H. C. et al. Exploitation of a Rod-Shaped, Acid-Labile Curcumin-Loaded Polymeric Nanogel System in the Treatment of Systemic Inflammation. *Mater. Sci. Eng. C.* **133**, 112597 (2021).
65. Blevins, H. M., Xu, Y., Biby, S. & Zhang, S. The NLRP3 Inflammasome Pathway: A Review of Mechanisms and Inhibitors for the Treatment of Inflammatory Diseases. *Front. Aging Neurosci.* **14**, 1–27 (2022).
66. Yu, T.-G. et al. Oligomeric States of ASC Specks Regulate Inflammatory Responses by Inflammasome in the Extracellular Space. *Cell Death Discov.* **9**, 142 (2023).
67. Zhao, Y. et al. A Virulent Bacillus Cereus Strain from Deep-Sea Cold Seep Induces Pyroptosis in a Manner That Involves NLRP3 Inflammasome, JNK Pathway, and Lysosomal Rupture. *Virulence* **12**, 1362–1376 (2021).
68. Mathur, A. et al. Clostridium Perfringens Virulence Factors Are Nonredundant Activators of the NLRP 3 Inflammasome. *EMBO Rep.* 1–20. https://doi.org/10.15252/embr.202254600 (2023).
69. Antushevich, H. Interplays between Inflammasomes and Viruses, Bacteria (Pathogenic and Probiotic), Yeasts and Parasites. *Immunol. Lett.* **228**, 1–14 (2020).
70. Campden, R. I. & Zhang, Y. The Role of Lysosomal Cysteine Cathepsins in NLRP3 Inflammasome Activation. *Arch. Biochem. Biophys.* **670**, 32–42 (2019).
71. Jing, W., Lo Pilato, J., Kay, C., Man, S. M. Activation Mechanisms of Inflammasomes by Bacterial Toxins. *Cell. Microbiol.* **23** https://doi.org/10.1111/cmi.13309 (2021).
72. Mercer, J. & Helenius, A. Virus Entry by Macropinocytosis. *Nat. Cell Biol.* **11**, 510–520 (2009).
73. Feng, X. & Junsheng, Y. Lysosomal Calcium in Neurodegeneration. *Messenger (Los Angel)* **5**, 56–66 (2017).
74. Brough, D. et al. Ca 2+ Stores and Ca 2+ Entry Di Erentially Contribute to the Release of IL-1B and IL-1α from Murine Macrophages. *J. Immunol.* **170**, 3029–3036 (2003).
75. Yaron, J. R. et al. K+ Regulates Ca2+ to Drive Inflammasome Signaling: Dynamic Visualization of Ion Flux in Live Cells. *Cell Death Dis.* **6**, 1–11 (2015).
76. Qiu, Y. et al. Mitochondrial DNA in NLRP3 Inflammasome Activation. *Int. Immunopharmacol.* **108**, 108719 (2022).
77. Heid, M. E. et al. Mitochondrial Reactive Oxygen Species Induces NLRP3-Dependent Lysosomal Damage and Inflammasome Activation. *J. Immunol.* **191**, 5230–5238 (2013).
78. Kumrungsee, T., Zhang, P., Yanaka, N., Suda, T. & Kato, N. Emerging Cardioprotective Mechanisms of Vitamin B6: A Narrative Review. *Eur. J. Nutr.* **61**, 605–613 (2022).
79. Teng, Y. et al. The Emerging Roles of Pyroptosis, Necroptosis, and Ferroptosis in Non-Malignant Dermatoses: A Review. *J. Inflamm. Res.* **16**, 1967–1977 (2023).
80. Mikhaylov, D., Hashim, P., Nektalova, T. & Goldenberg, G. Systemic Psoriasis Therapies and Comorbid Disease in Patients with Psoriasis: A Review of Potential Risks and Benefits. *J. Clin. Aesthet. Dermatol* **12**, 46–54 (2019).
81. Jiao, Y. et al. Discovery of a Novel and Potent Inhibitor with Differential Species-Specific Effects against NLRP3 and AIM2 Inflammasome-Dependent Pyroptosis. *Eur. J. Med. Chem.* **232**. https://doi.org/10.1016/j.ejmech.2022.114194 (2022).
82. Liu, T. et al. Evaluation of the Anti-Biofilm Effect of Poloxamer-Based Thermoreversible Gel of Silver Nanoparticles as a Potential Medication for Root Canal Therapy. *Sci. Rep.* **11**, 1–16 (2021).
83. Cook, M. T., Haddow, P., Kirton, S. B., McAuley, W. J. Polymers Exhibiting Lower Critical Solution Temperatures as a Route to Thermoreversible Gelators for Healthcare. *Adv. Funct. Mater.* **31** https://doi.org/10.1002/adfm.202008123 (2021).
84. Fakhari, A., Corcoran, M. & Schwarz, A. Thermogelling Properties of Purified Poloxamer 407. *Heliyon* **3**, e00390 (2017).
85. ter Horst, B. et al. A Gellan-Based Fluid Gel Carrier to Enhance Topical Spray Delivery. *Acta Biomater.* **89**, 166–179 (2019).
86. Chang, Y. et al. A Systematic SPR Study of Human Plasma Protein Adsorption Behavior on the Controlled Surface Packing of Self-Assembled Poly(Ethylene Oxide) Triblock Copolymer Surfaces. *J. Biomed. Mater. Res. - Part A* **93**, 400–408 (2010).
87. Binder, L., Mazál, J., Petz, R., Klang, V. & Valenta, C. The Role of Viscosity on Skin Penetration from Cellulose Ether-Based Hydrogels. *Ski. Res. Technol.* **25**, 725–734 (2019).
88. Liao, W. & Aranson, I. S. Viscoelasticity Enhances Collective Motion of Bacteria. *PNAS Nexus* **2**, 1–10 (2023).
89. Desmet, E., Ramadhas, A., Lambert, J. & Van Gele, M. In Vitro Psoriasis Models with Focus on Reconstructed Skin Models as Promising Tools in Psoriasis Research. *Exp. Biol. Med.* **242**, 1158–1169 (2017).
90. Bochénska, K., Smolińska, E., Moskot, M., Jakóbkiewicz-Banecka, J. & Gabig-Cimińska, M. Models in the Research Process of Psoriasis. *Int. J. Mol. Sci.* **18**, 1–17 (2017).
91. Neil, J. E., Brown, M. B. & Williams, A. C. Human Skin Explant Model for the Investigation of Topical Therapeutics. *Sci. Rep.* **10**, 1–8 (2020).
92. Ahn, M. et al. 3D Biofabrication of Diseased Human Skin Models in Vitro. *Biomater. Res.* **27**, 1–13 (2023).

93. Schön, M. P., Manzke, V. & Erpenbeck, L. Animal Models of Psoriasis—Highlights and Drawbacks. *J. Allergy Clin. Immunol.* **147**, 439–455 (2021).
94. Garzorz-Stark, N. et al. Toll-like Receptor 7/8 Agonists Stimulate Plasmacytoid Dendritic Cells to Initiate TH17-Deviated Acute Contact Dermatitis in Human Subjects. *J. Allergy Clin. Immunol.* **141**, 1320–1333.e11 (2018).
95. Elias, M. et al. IL-36 in Chronic Inflammation and Fibrosis - Bridging the Gap? *J. Clin. Invest.* **131** https://doi.org/10.1172/JCI144336 (2021).
96. Gangwar, R. S., Gudjonsson, J. E. & Ward, N. L. Mouse Models of Psoriasis: A Comprehensive Review. *J. Invest. Dermatol.* **142**, 884–897 (2022).
97. Bhalerao, J. Bowcock, A. M. The Genetics of Psoriasis: A Complex Disorder of the Skin and Immune System. *Hum. Mol. Genet.* **7**, 1537–1545 (1998).
98. Bromley, S. K., Larson, R. P., Ziegler, S. F. & Luster, A. D. IL-23 Induces Atopic Dermatitis-Like Inflammation Instead of Psoriasis-Like Inflammation in CCR2-Deficient Mice. *PLoS One* **8**, 1–10 (2013).
99. Swindell, W. R. et al. Imiquimod Has Strain-Dependent Effects in Mice and Does Not Uniquely Model Human Psoriasis. *Genome Med* **9**, 1–21 (2017).
100. Jiang, W. et al. A Toll-like Receptor 7, 8, and 9 Antagonist Inhibits Th1 and Th17 Responses and Inflammasome Activation in a Model of IL-23-Induced Psoriasis. *J. Invest. Dermatol.* **133**, 1777–1784 (2013).
101. Miller, L. S. Toll-Like Receptors in Skin. *Adv. Dermatol.* **24**, 71–87 (2008).
102. von Stebut, E. et al. IL-17A in Psoriasis and Beyond: Cardiovascular and Metabolic Implications. *Front. Immunol.* **10**, 1–15 (2020).
103. Brembilla, N. C., Senra, L., Boehncke, W. H. The IL-17 Family of Cytokines in Psoriasis: IL-17A and Beyond. *Front. Immunol.* **9**. https://doi.org/10.3389/fimmu.2018.01682 (2018).
104. Mosca, M. et al. The Role of IL-17 Cytokines in Psoriasis. *Immuno-Targets Ther.* **10**, 409–418 (2021).
105. Branisteanu, D. et al. Update on the Etiopathogenesis of Psoriasis (Review). *Exp. Ther. Med.* **23**, 1–13 (2022).
106. Chan, J. R. et al. IL-23 Stimulates Epidermal Hyperplasia via TNF and IL-20R2-Dependent Mechanisms with Implications for Psoriasis Pathogenesis. *J. Exp. Med.* **203**, 2577–2587 (2006).
107. De, R. & Mignogna, C. The Histopathology of Psoriasis. *Reumatismo* **59**, 46–48 (2007).
108. Lo, Y. H. et al. Galectin-8 Is Upregulated in Keratinocytes by IL-17A and Promotes Proliferation by Regulating Mitosis in Psoriasis. *J. Invest. Dermatol.* **141**, 503–511.e9 (2021).
109. Yazici, A. C. et al. The Changes in Expression of ICAM-3, Ki-67, PCNA, and CD31 in Psoriatic Lesions before and after Methotrexate Treatment. *Arch. Dermatol. Res.* **297**, 249–255 (2005).
110. Lee, H. J., Kim, M. Challenges and Future Trends in the Treatment of Psoriasis. *Int. J. Mol. Sci.* **24** https://doi.org/10.3390/ijms241713313 (2023).
111. Woo, Y. R., Park, C. J., Kang, H. & Kim, J. E. The Risk of Systemic Diseases in Those with Psoriasis and Psoriatic Arthritis: From Mechanisms to Clinic. *Int. J. Mol. Sci.* **21**, 1–27 (2020).
112. Thatiparthi, A., Martin, A., Liu, J. & Wu, J. Risk of Skin Cancer with Phototherapy in Moderate-to- Severe Psoriasis. *J. Clin. Aesthet. Dermatol.* **15**, 68–75 (2022).
113. Elmets, C. A. et al. Joint AAD–NPF Guidelines of Care for the Management and Treatment of Psoriasis with Topical Therapy and Alternative Medicine Modalities for Psoriasis Severity Measures. *J. Am. Acad. Dermatol.* **84**, 432–470 (2021).
114. Coondoo, A., Phiske, M., Verma, S. & Lahiri, K. Side-Effects of Topical Steroids: A Long Overdue Revisit. *Indian Dermatol. Online J.* **5**, 416 (2014).
115. Stacey, S. K. & McEleney, M. Topical Corticosteroids: Choice and Application. *Am. Fam. Physician* **103**, 337–343 (2021).
116. Hwang, J. & Lio, P. A. Topical Corticosteroid Withdrawal ('Steroid Addiction'): An Update of a Systematic Review. *J. Dermatol. Treat.* **33**, 1293–1298 (2022).
117. Barrea, L. et al. Vitamin D and Its Role in Psoriasis: An Overview of the Dermatologist and Nutritionist. *Rev. Endocr. Metab. Disord.* **18**, 195–205 (2017).
118. Nicholas Brownstone, M. Psoriasis Therapies in 2024 and Beyond. *Dermatology Times*. https://www.dermatologytimes.com/view/psoriasis-therapies-in-2024-and-beyond (accessed 2024-04-07).
119. Guo, J. et al. Signaling Pathways and Targeted Therapies for Psoriasis. *Signal Transduct. Target. Ther.* **8** https://doi.org/10.1038/s41392-023-01655-6 (2023).
120. Surve, D. H., Jirwankar, Y. B., Dighe, V. D., Jindal, A. B. Long-Acting Efavirenz and HIV-1 Fusion Inhibitor Peptide Co-Loaded Polymer-Lipid Hybrid Nanoparticles: Statistical Optimization, Cellular Uptake, and In Vivo Biodistribution. *Mol. Pharm.* **17** https://doi.org/10.1021/acs.molpharmaceut.0c00773 (2020).
121. Surve, D. H. & Jindal, A. B. Development of Cationic Isometamidium Chloride Loaded Long-Acting Lipid Nanoformulation: Optimization, Cellular Uptake, Pharmacokinetics, Biodistribution, and Immunohistochemical Evaluation. *Eur. J. Pharm. Sci.* **167**, 106024 (2021).
122. Fish, A. & Kulkarni, A. Flow-Induced Shear Stress Primes NLRP3 Inflammasome Activation in Macrophages via Piezo1. *ACS Appl. Mater. Interf.* **16**, 4505–4518 (2024).


## Acknowledgements

This work was financially supported by the American Cancer Society Research Scholar Grant (RSG-19-009-01-CDD) and National Science Foundation CAREER Award (2142917) to A.K. This investigation was supported in part by National Research Service Award T32 GM135096 from the National Institutes of Health to A.F. A.L. was supported by grants from the NIH (U01CA265709 and T32GM139789) and a Spaulding Smith fellowship. S.R.P. was supported by a grant from the Jayne Koskinas and Ted Giovanis Foundation for Health and Policy and the NSF (DMR1905559). We would like to thank the Biophysical Characterization Core at the Institute for Applied Life Sciences (IALS), the University of Massachusetts Amherst, for lending their expertise regarding characterization experiments. We would also like to thank the Light Microscopy Core Facility at the University of Massachusetts Amherst for their help and consultation while performing confocal imaging. All institutional and national guidelines for the care and use of laboratory animals were followed and approved by the University of Massachusetts Amherst Institutional Use and Care of Animals Committee. All the visual figures were created with Biorender.com.

## Author contributions

D.S. and A.K. conceived the idea for this project; D.S. synthesized and characterized the lipid nanoparticles and polymeric scaffold; D.S., A.F., M.D. and A.P. performed the in vitro and in vivo experiments; A.L. performed the rheological characterization of the scaffold; S.P. performed the microscopic analysis for IHC and H&E stained sections. D.S. and A.K. wrote the manuscript and received comments and edits from all the authors; S.R.P. reviewed and edited the manuscript; A. K. and S.R.P. supervised the research; A.F. and M.D. contributed equally.

## Competing interests

D.S. and A.K. has filed a patent application on this research. The remaining authors declare no competing interests.

## Additional information

**Supplementary information** The online version contains supplementary material available at https://doi.org/10.1038/s41467-024-53396-x.

**Correspondence** and requests for materials should be addressed to Ashish Kulkarni.

**Peer review information** *Nature Communications* thanks Kohsuke Tsuchiya and the other, anonymous, reviewers for their contribution to the peer review of this work. A peer review file is available.